Dear Alison Anders,

5 thank you for your constructive and insightful comments which we feel helped to improve the manuscript.

We (i) uploaded a revised version of the manuscript (one version with markups showing revisions and responses to minor comments, the other with a clean layout), (ii) posted a new author's comment to inform on general amendments in the manuscript, and (iii) below provide a point-by-point response to your comments. Our response is structured as follows: (1)
10 referee comment and (2) author's response including direct references to manuscript changes.

(1) I would encourage the authors to use the observations to more carefully test some hypotheses on what controls the rate of cirque-headwall rockfalls. Specifically, please elaborate on the pattern of rockfall with orientation. The bedrock is described as having prominent cleavage to the NE and lots of jointing (without orientations provided).
15 The majority of rockfalls are on NW or N facing slopes - which is attributed to specific locations? Perhaps the figure could be clarified to differentiate between rockfalls in different locations. Can this be clarified?
(2) We added information on discontinuities/jointing to the study site description (see Sect. 2 and new Fig. 4), and added a new subchapter in which we elaborate on the pattern of rockfall with orientation (see Sect. 4.4 Directional Rockfall Distribution). We furthermore added a paragraph on the sectoral rockfall distribution to the beginning of
20 the discussion (Sect. 5)

(1) There are faults in the vicinity of the major rockfalls? Can those faults be shown on the images?
(2) Faults/Weakness zones are now displayed on Fig. 4, 7 and 8 which were added to the manuscript.

25 (1) Can joint/fracture spacing be quantified on the different faces? (Perhaps using the existing Lidar data?)
(2) The quantification of joint/fracture spacing would require higher data resolution. We added new figures (Fig. 4, 7 and 8) to visualise weakness zones in more detail and added a verbal description of zones with increased rockfall activity to Sect 4.2.

30 (1) Is there a difference in the thickness of the rockfalls with orientation (or a pattern related to location)?
(2) We expanded Sect. 4.6 (Rockfall Failure Depths) and added a classification of rockfall failure depth by slope aspect (Table 2).

(1) I would expect that microclimates would impact the rate of development of the active layer and the ultimate
35 thickness of the active layer - and I would also expect that the microclimates might be largely controlled by aspect. Could the diurnal/seasonal temperature variations be modeled for the rockwall faces? Are any instrumental temperature data available?
(2) We added new (instrumental) temperature data to the manuscript, which includes (i) a set of unprecedented rock temperature data from the Randkluft, and (ii) datasets from 'cold' N-facing sections and 'warm' ESE-facing
40 sections to compare the spectrum of seasonal variations. Data acquisition and measurement sites are described in Sect. 3.2, results are described in Sect. 4.7, and discussed in Sect. 5.1 and 5.2.

(1) Basically, I think that this data set could be probed in more detail to discern the influence of structure (jointing, foliation, faults) vs. climate in the rates and size of rockfalls. Doing so has the potential to increase the impact and
45 significance of the paper.
(2) By adding the above mentioned information on bedrock temperature and structural weaknesses we hope to give a more rounded picture that allows better differentiation between the influence of structure vs.

Response to RC2 (Robert Kenner):

Dear Robert Kenner,

thank you for your constructive and insightful comments which we feel helped to improve the manuscript.

55 We (i) uploaded a revised version of the manuscript (one version with markups showing revisions and responses to minor comments, the other with a clean layout), (ii) posted a new author's comment to inform on general amendments in the manuscript, and (iii) below provide a point-by-point response to your comments. Our response is structured as follows: (1) referee comment, (2) author's response including direct references to manuscript changes.

60 (1) You did a good job in estimating the accuracy of your measurements. However, I miss something similar for the statistics. Some of the statistical analysis are based on very small sample sizes or are strongly influenced by single events. I wonder if all this is significant and would appreciate something like a sensitivity analysis.

(2) Following your suggestion we added a sensitivity analysis to the manuscript (see last two paragraphs of Sect. 4.5 and new Fig. 12). The sensitivity analysis is described in full detail in the companion paper.

65

(1) The second part of 5.1 when you describe subglacial rock fracturing is not convincing. First you say, that there is no active layer here (I agree with Jan that there is one at least in the upper meters but likely clearly thinner than above the glacier line) and that the melt water refreezes at the surface but then you write, that large amounts of melt water 70 enables frost cracking. How should that be possible from the surface? Important for subglacial rock weathering within a Bergschrund is probably ice-segregation but this is not even mentioned.

(2) We added a multi-year temperature dataset from the Randkluft to describe its thermal regime in more detail. Data acquisition and measurement sites are described in Sect. 3.2, results are described in Sect. 4.7, and discussed in Sect. 5.1 and 5.2. Our measurements/observations suggest sustained freezing and ample water supply inside the Randkluft 75 at the same time (during summer) – two key requirements for ice segregation (and thus for frost cracking) (see also analyses of Sanders et al. 2012, Alley et al. 2019, Evans et al. 2020 who all assume enhanced frost cracking inside the Randkluft). We feel that some confusion was arising from our use of the term "subcritical fracture propagation" (which results from ice segregation). We adapted the terminology to emphasise the role of ice segregation more clearly (see amendments in Sect. 5.1).

80 (1) Section 5.1 gives the subliminal impression that rock wall erosion or at least rock wall weakening is higher in the Randkluft than on a not glacially affected rock. This is however the major question which is not satisfyingly discussed: If I imagine a constant slope and put a glacier at its foot and than I wait for 50'000 years, the rock wall is commonly steeper in the area around the Bergschrund after this time. These steep belts are called Schrundlines and you made a similar observation at your site. Now where does this steepening come from? Is it because the glacier erodes the foot 85 of the rock wall below the Randkluft or does the glacier in contrast protect the rock wall from temperature forcing and decelerates rock erosion while higher erosion rates above the randkluft cause a flattening of the rock wall? Obviously, erosion rates increase after glaciation right? But what is higher? Subglacial erosion or erosion in summit regions not affected by glaciation? Perhaps you can discuss this very basic but unsolved question.

(2) Following your suggestions we added a brief discussion on the implications for (subglacial) headwall retreat. See last 90 paragraph of Sect. 5.1.

(1) I am fundamtally not convinced by these error specification and consider them as much to low and highly theoretical. 1.5 m3 is already the talus which is deposited within failiure scar of a rock fall.

(2) Gaussian error propagation brought the error down to unrealistically low values and was therefore replaced. We 95 updated the error calculation accordingly (which now yields an average relative error of 5.5 %), which is described in Sect. 3.1.2.

References

100   Alley RB, Cuffey KM, Zoet LK (2019). Glacial erosion: status and outlook. Annals of Glaciology 60(80), 1–13. https://doi.org/10.1017/aog.2019.38

Evans, IS (2020). Glaciers, rock avalanches and the 'buzzsaw' in cirque development: Why mountain cirques are of mainly glacial origin. Earth Surface Processes and Landforms, DOI: 10.1002/esp.4810.

Sanders, J. W., Cuffey, K. M., Moore, J. R., MacGregor, K. R., and Kavanaugh, J. L.: Periglacial weathering and headwall
105   erosion in cirque glacier bergschrunds, GEOLOGY, 40(9), 779-782, 2012.

Response to SC1 (Jan Beutel):

Dear Jan Beutel,

thank you for your constructive and insightful comments which we feel helped to improve the manuscript.

We (i) uploaded a revised version of the manuscript (one version with markups showing revisions and responses to minor comments, the other with a clean layout), (ii) posted a new author's comment to inform on general amendments in the manuscript, and (iii) below provide a point-by-point response to your comments. Our response is structured as follows: (1) referee comment, (2) author's response including direct references to manuscript changes.

(1) Specifically I am lacking a pertinent discussion as to the accuracy and validity of your quantitative analysis presented. In no way do I doubt your figures, but in the form they are presented it remains largely unclear how large or small your errors presented are w.r.t. the state of the art and what this errors depend on. I am especially worried since there is no apparent attempt to validate at least part of the figures presented. is it possible to manually cross check the volumes presented with photographs, site visits, deposits on the glacier surface such as seen in fig 4/KNW and KN?

(2) We expanded the description of the error calculation (Sect. 3.1.2) and provided additional information (Sect. 4.2) and figures (Fig. 7 and 8) to validate our observations/analyses.

(1) I am missing a detailed discussion of the exposition and the role of radiation/shading. can you add into figure 5 (polar plot) at which expositions you actually have rock walls in your portfolio and possibly also how much? You show altitude in great detail (fig 6) but little is shown w.r.t. south/north facing. Also your discussion of aggrading/degrading permafrost/active layer is weak and in parts not concise w.r.t. the influence of radiation and the stresses originating from it.

(2) Following your suggestions we added a new subchapter that elaborates on the pattern of rockfall with orientation (see Sect. 4.4 Directional Rockfall Distribution). We furthermore added a paragraph on the sectoral rockfall distribution to the beginning of the discussion (Sect. 5).

(1) In section 5 you discuss that groups of rockfall can be observed e.g. near structural weaknesses or in immediate proximity of the glacier surface. It would be very interesting to see this observation also in your evidence. Can you point out such weaknesses in the topography/photos? Can you point out such hot spots in there as well. Fig. 4 only shows the approximate distribution and size of the observations. But if you are really able to bin these into classes and connect them with properties of the environment, you should really show evidence for that. Maybe only in the form of a spot check and not a total cumulative analysis but without further backing this claim is hard to make. A more detailed discussion and evidence of fracture/weaknesses existing in the Kitzsteinhorn rockwalls would be helpful.

(2) We expanded the study site description (Sect. 2) which now includes information on the dominant discontinuity directions. We furthermore added new content and new figures (Fig. 7 and 8) to Sect. 4.2 to demonstrate the rockfall concentration in weakness zones.

(1) I am not convinced of the discussion of the randkluft as you present it. To my understanding the key property of such deep reaching voids, typically found at the upper boundaries of glacier cirques (not just in the Alps) is that there is no continuous physical contact between ice and ground (rock). This means that there is no mass loading with ice or water pressure and the rock surface is largely exposed to air. So in effect the rock walls are "free standing" compared to vertical (or steep) rock parts that are completely encased in ice. Due to this missing mass loading and the missing water pressure the hydraulic regime changes (see e.g. Simon Loew et al Aletsch Glacier etc.).
Due to the Randkluft reaching deep this is probably the case since a long time - a very long time. Concerning the air and the governing temperature regime I disagree that there is no active layer. It may not be very significant but your

4

claim about ice cover in mid-October is not convincing, knowing that mid summer is in the end of June and that there is a lot of running water traversing these rock faces from spring (snowmelt) to fall bringing a lot of thermal energy deep into these rock faces below the glacier surface. I rather think that the active layer (and permafrost) regime is of very different properties (temporal, dimensional as well as thermal) as in free surfaces. So maybe you can add thermal data to back up your evidence. In a minimum this should be MAAT, MAGST etc. a discussion of north/south, shaded vs. unshaded etc.

(2) Following your suggestions we added a multi-year temperature dataset from the Randkluft to describe its thermal regime in more detail. Data acquisition and measurement sites are described in Sect. 3.2, results are described in Sect. 4.7, and discussed in Sect. 5.1 and 5.2.

(1) Figure 2: Possibly this figure could be augmented by an even newer picture (end of the study period) to show explicitly the deglaciation that took place during the study period. Also, can you quantify this deglaciation somehow?

(2) We added a new subchapter (Sect. 2.1 Deglaciation) to discuss deglaciation during the study period more explicitly. We furthermore reconstructed the approximate level of the glacier surface from an aerial photo from 1953 (see Fig. 1 and new Fig. 3) and added a new table (Table S8) to the supplement.

(1) Table 2: Rather than repeating the sales brochure of Riegl please specify the settings used for obtaining your data. The general specs of this instruments are known/accessible through the manufacturer to everyone.

(2) Table 2 was removed and information was added to the text. Detailed information on data acquisition parameters are given in Table S2.

(1) Section 3.2: It would help if you give a short synopsis of the algorithms used (M3C2) and not only list benefits similar as how you briefly explain ICP above.

(2) Following your suggestion we provided a synopsis of the algorithm used (new Sect. 3.1.2).

(1) Availability of the data: Is the LIDAR (airborne and terrestrial) available? or can it be made available

(2) The terrestrial LiDAR data is available on request.

(1) Section 4.1: What is the detection limit mentioned? And how is this error determined? can you explain what influences this error (besides the size of the rockfall)? – You mention a theoretical discrepancy w.r.t. the detection. can you please detail here? And besides theory, what does it mean in practice for your study?

(2) We renamed Sect. 4.1. and modified the paragraph. Please also refer to Sect. 3.1.2 where the error calculation is now described in more detail. The error calculation of the M3C2 does not discern between different error sources but instead gives a cumulative error (that factors in all error sources).

(1) Figure 3: What are the two lines? The correlations? Please explain this in detail.

(2) The lines represent the regression lines of the two distributions (all rockfalls; rockfalls > 0.1 m³). We updated the caption.

(1) Section 4.2: Errors of +/- 1.5 m^3 and 1.3m^3 respectively. How sure are you? How did you validate this.

(2) Gaussian error propagation brought the error down to unrealistically low values and was therefore replaced. We updated the error calculation accordingly (which now yields an average relative error of 5.5 %), which is described in Sect. 3.1.2.

(1) Page 12, L 276: You discuss an event that took place before your campaign. If there is a direct context with the observations during your campaign, please explain and back this up with data and plots. If not leave this out. the discussion here is only of a qualitative nature.

(2) The mentioned past event seems to directly control current rockfall activity in the investigated rockwall. Despite the occurrence prior to the start of our monitoring campaign we believe it is justified to mention said event as it helps the reader interpret the observed patterns. We rephrased the relevant passages and hope it is clearer now (Sect. 4.2).

210

(1) Figure 8: Normally CDF functions are given normalized to 100% and not in absolute numbers. Maybe you can also add the thermal data you have to this plot, although clearly one borehole somewhere else is only of limited use in the discussion (you discuss this somewhere later).

(2) We modified the plot. The plot is now given normalized to 100 % and the seasonal maximum of the active layer is indicated.

215

(1) Page 14, L 320: I do not see what hinders debuttressing in this case.

(2) Due to the existence of a Randkluft (air-/snow-filled void) there is no direct contact between the glacier and its headwall (at least down to a certain depth), the glacier does not function as a buttress. Along the no-contact zone we therefore consider debuttressing as irrelevant.

220

6

Current glacier recession causes significant rockfall increase:
The immediate paraglacial response of deglaciating cirque walls

Ingo Hartmeyer[1], Robert Delleske[1], Markus Keuschnig[1], Michael Krautblatter[2], Andreas Lang[3], Lothar Schrott[4], Jan-Christoph Otto[3]

[1]GEORESEARCH Research Institute, Wals, 5071, Austria
[2]Chair of Landslide Research, Technical University of Munich, Munich, 80333, Germany
[3]Department of Geography and Geology, University of Salzburg, Salzburg, 5020, Austria
[4]Department of Geography, University of Bonn, Bonn, 53115, Germany

Correspondence to: Ingo Hartmeyer (ingo.hartmeyer@georesearch.ac.at)

Abstract. In the European Alps almost half the glacier volume disappeared over the past 150 years. The loss is reflected in glacier retreat and ice surface lowering even at high altitude. In steep glacial cirques surface lowering exposes rock to atmospheric conditions probably for the very first time in ~~many~~ several millennia. Instability of rockwalls has long been identified as one of the direct consequences of deglaciation, but so far cirque-wide quantification of rockfall at high-resolution is missing. Based on terrestrial LiDAR a rockfall inventory for the permafrost-affected rockwalls of two rapidly deglaciating cirques in the Central Alps of Austria (Kitzsteinhorn) is established. Over six-years (2011-2017) 78 rockwall scans were acquired to generate data of high spatial and temporal resolution. 632 rockfalls were registered ranging from 0.003 to 879.4 m³, mainly originating from pre-existing structural rock weaknesses. 60 % of the rockfall volume detached from less than ten vertical meters above the glacier surface, indicating enhanced rockfall activity over tens of years following deglaciation. Debuttressing seems to play a minor effect only. Rather, preconditioning is assumed to start inside the Randkluft (~~gap~~void between cirque wall and glacier) where measured sustained freezing and ample supply of liquid water likely cause enhanced physical weathering and high ~~plucking~~ quarrying stresses. Following deglaciation, pronounced thermomechanical strain is induced and an active layer penetrates into the formerly perennially frozen bedrock. These factors likely cause the observed paraglacial rockfall increase close to the glacier surface. This paper, the first of two companion pieces, presents the most extensive dataset of high-alpine rockfall to date and the first systematic documentation of a cirque-wide erosion response of glaciated rockwalls to recent climate warming.

1 Introduction

High-alpine, glacial environments are severely affected by recent climate warming (WGMS, 2017). This is especially true for the European Alps, where mean temperature rise over the last 150 years more than doubled the global mean (Böhm, 2012) and over this period approximately 50 % of the glacier volume has disappeared (Haeberli et al., 2007). Glacier retreat rates increased since the 1980s and have been exceeding historical precedents in the early 21st century (Zemp et al., 2015). The consequences of these changes are most visible in lower lying glacierized cirques where ice-surface lowering in the ablation

Kommentiert [IH1]: Modified following suggestions by RC2 (R. Kenner). See first paragraph of introduction for further explanation.

Kommentiert [IH2]: Following suggestions by Alley et al. 2019 (p. 5) we use the term 'quarrying' instead of 'plucking'.

Reference:
Alley RB, Cuffey KM, Zoet LK (2019). Glacial erosion: status and outlook. Annals of Glaciology 60(80), 1–13. https://doi.org/10.1017/aog.2019.38

Kommentiert [IH3]: Added to inform the reader about the companion paper.

area is particularly apparent (Kaser et al., 2006; Pelto, 2010) and exposes cirque walls to the atmosphere ~probably for the first time in ~~many~~ several millennia ~~(Hormes et al., 2001)~~. Paleoclimatic studies assume that glaciers are currently shrinking to extents that are unprecedented since the Medieval (~ 1 ka ago) or Roman Warm Periods (~ 2 ka ago) (Holzhauser et al., 2005; Jörin et al., 2006), or more likely, since the mid-Holocene Warm Period (~ 5 ka ago) (Jörin et al., 2008; Auer et al., 2014; Solomina et al., 2015).

Rockwall characteristics strongly depend on preconditioning stress fields (Krautblatter and Moore, 2014). Especially parameters such as fracture density and orientation are first order controls on rock slope erosion (Sass, 2005; Moore et al., 2009). Glacial oversteepening increases the stress regime acting within cirque walls and promotes rock slope failures at various scales (Ballantyne, 2002; de Haas et al., 2015). Ice surface lowering alters ground thermal conditions (Wegmann et al., 1998) modifies pre-existing slope stresses (Augustinus, 1995; Leith et al., 2014) and therefore potentially causes local instability and elevated mass wasting activity. This has significant implications for risk management in high-alpine environments – especially when considering the growing popularity of glacier tourism (Fischer et al., 2011a; Purdie, 2013). Steep gradients (due to ~~Gg~~lacial oversteepening) ~~of~~ in the surrounding rockwalls and the low friction on the glacier surface ~~often results~~ both promote ~~in~~ long rockfall runouts underneath cirque walls (Schober et al., 2012) putting nearby infrastructure at risk. Continued climate warming is expected to exacerbate this issue, making long-term rockwall monitoring an essential prerequisite for rockfall risk assessment in glacial environments (Stoffel and Huggel, 2012).

Frost action is considered a key agent in preparing and triggering high-alpine rockfall (Draebing and Krautblatter, 2019) and a major driver of rock slope erosion in cold environments (e.g. Hales and Roering, 2009). Only recently a number of studies demonstrated cirque wall retreat rates exceeding rates of glacial incision, underlining the contribution of frost weathering to the shaping of 'glacial' landscapes (Oskin and Burbank, 2005; Naylor and Gabet, 2007; Scherler et al, 2011). Frost weathering processes encompass volumetric ice expansion and ice segregation which are theoretically able to produce pressures exceeding the tensile strength of rocks (Matsuoka and Murton, 2008; Hallet et al., 1991). Volumetric expansion results from freezing of in-situ water and requires high water saturation and extreme cooling rates (Walder and Hallet, 1986; Matsuoka and Murton, 2008). Ice segregation causes cryosuction-induced migration of unfrozen water toward freezing fronts (Walder and Hallet, 1985) and is effective in hard, low-porosity rock at a wide range of sustained sub-zero temperatures (Girard et al., 2013; Duca et al., 2014; Murton et al., 2016). Recent lab studies highlight the importance of fatigue damage under different frost weathering regimes and in different rock types and indicate that subcritical crack propagation plays a key role in the generation of rockfalls in periglacial environments (Jia et al., 2015; Jia et al., 2017).

Rockfall or rock slope failures that are spatiotemporally related to the transition from glacial conditions to non-glacial conditions have been termed 'paraglacial' (McColl, 2012). The paraglacial concept incorporates processes, materials and landforms that are directly conditioned by former glaciation and deglaciation (Church and Ryder, 1972; Ballantyne, 2002). Studies on paraglacial rock slope readjustment often focus on enhanced rates of geomorphic activity after/during deglaciation mainly on rare high-magnitude slope failures. Frequent low-magnitude failure patterns have received comparably little

Kommentiert [IH4]: Modified following suggestion by RC2 (R. Kenner):

RC2 (R. Kenner) wrote:
"I consider this statement as problematic. Hormes et al. concludes that glacier extents around 1-1.5k years ago were smaller than in 2001 This is ony ONE millenia. Moreover they did not investigated glacier levels at cirque walls but glacier termini and as said before the study is pretty old for such dynamic changes."

Kommentiert [IH5]: Modified following suggestion by RC2 (R. Kenner):

RC2 (R. Kenner) wrote:
"Not clear how this influences run out distances."

attention. Numerous studies on paraglacial bedrock erosion have focused on Late Pleistocene to Holocene timescales that relate to glacier retreat from Last Glacial maximum (LGM) positions. Relevant studies include extensive mapping of slope instabilities (Allen et al., 2010), terrestrial cosmogenic nuclide dating of post-glacial rock slope failures (Cossart et al. 2008, Ballantyne et al., 2014), effects of glacial debuttressing (McColl and Davies, 2012) and numerical modelling of fracture initiation and propagation during glacial (un)loading (Grämiger et al., 2017).

On a more recent time scale the effects of glacier shrinkage from Little Ice Age (LIA) limits and increased mass wasting activity are unravelled using field mapping (Deline, 2009), photograph comparisons (Ravanel and Deline, 2010), GIS analyses (Holm et al., 2004) and historical documentation (Noetzli et al., 2003). Paraglacial adjustment to the most recent episode of glacial recession – i.e. the dramatic glacier retreat observed over the past few decades – has so far only marginally been addressed. In the Alps, singular, high-magnitude events were examined in the Mont Blanc Massif, France (Deline et al., 2008), at the Piz Kesch, Switzerland (Phillips et al., 2017) and adjacent to the Aletsch Glacier, Switzerland (Manconi et al., 2018) and have at least partially been attributed to current glacier melting. Quantitative studies of lower magnitude paraglacial rockfalls are rare and include a detailed topographic study of rock and ice avalanches in the Monte Rosa east-face, Italy (Fischer et al. 2011b), a four-year time series on a paragneiss ridge at the Gemsstock ski area, Switzerland (Kenner et al., 2011), a two-year monitoring from the Tour Ronde east-face, France (Rabatel et al., 2008), and slope stability surveys from the surroundings of the Refuge des Cosmiques, France (Ravanel et al., 2013).

Quantification of paraglacial rockfall release over larger surfaces and over several years is missing – in large parts due to the harsh, high-alpine environmental conditions – and effectively hinders evaluating the impacts of current glacier retreat on rockfall occurrence. Using data from a six-year terrestrial LiDAR monitoring campaign (2011-2017), we present a rockfall inventory from the Central Alps of Austria that is unique for high-alpine study areas in spatial and temporal extent, and level of detail. We (i) systematically quantify rockfall in two neighbouring, glacial cirques, (ii) reveal significantly increased (paraglacial) rockfall in recently deglaciated rockwall sections immediately above the current glacier surface, (iii) use a unique multiyear set of bedrock temperatures acquired inside the Randkluft to quantify thermal effects of deglaciation on adjacent rockwalls, and (iv~~iii~~) identify antecedent rockfall preparation inside the Randkluft (subcritical crack propagation driven by ice segregation, ~~plucking~~quarrying-related tensile stress) and subsequent deglaciation-induced thermal forcing as most likely causes for the observed glacier-proximal concentration of rockfall source areas.

Here, after documenting study area and method applied, an inventory of mass movements is presented. Data quality is analysed, spatial patterns of rockfall and rockfall failure depth are presented and causes of the observed rockfall patterns discussed. Magnitude-frequency relationships and rockwall retreat rates derived from this data are discussed in a companion study (Hartmeyer et al., 2020~~submitted~~).

9

2 Study Area

Two cirques located in the summit region of the Kitzsteinhorn (3,203 m a.s.l.), Hohe Tauern Range, Austria (Fig. 1), immediately northwest of the summit were selected for monitoring. Both cirques are occupied by the Schmiedingerkees glacier, which is home to Austria's oldest glacier ski-area. Since 2010 an extensive, multi-scale monitoring of permafrost-rockfall interaction ('Open-Air-Lab Kitzsteinhorn') (Keuschnig et al., 2015) includes several deep and shallow boreholes (Hartmeyer et al., 2012), two permanently installed electrical resistivity tomography profiles (Supper et al., 2014; Keuschnig et al., 2016), rock anchor load loggers (Plaesken et al., 2017), extensometers in fractures (Ewald et al., 2019) and several fully automated weather stations.

All rockwalls investigated here tower above the Schmiedingerkees glacier: the Kitzsteinhorn north-face (KN), the Kitzsteinhorn northwest-face (KNW), the Magnetkoepfl east-face (MKE), the Magnetkoepfl west-face (MKW) and the Maurergrat east-face (MGE). The total surface area of all rockwalls studied is 234,700 m² and with an area of 133,400 m² and a mean height of roughly 200 m KNW is the largest rockwall studied. Slope gradients within and across the rockwalls vary greatly. Typically, gradients increase towards the glacier surface, as is characteristic for cirque walls worldwide (Sanders et al., 2012). With 72 ° the steepest mean gradient occurs at MKE, followed by MKW (63 °), and KNW displays the lowest gradient (44 °) (Table 1 and Table S1).

Table 1: Selected morphometric parameters for all five investigated rockwalls.

	Area (m²)	Altitude (min/max) (m a.s.l.)	Avg. Height (m)	Avg. Slope (°)	Avg. Aspect (°)
Kitzsteinhorn north-face (KN)	23,500	2,921 / 3,060	~70	47	(N) 357
Kitzsteinhorn northwest-face (KNW)	133,400	2,768 / 3,203	~200	44	(NW) 322
Magnetkoepfl east-face (MKE)	11,100	2,853 / 2,953	~55	71	(E) 110
Magnetkoepfl west-face (MKW)	6,300	2,876 / 2,944	~35	63	(W) 268
Maurergrat east-face (MGE)	60,400	2,742 / 2,994	~55	61	(E) 086

The investigated rockwalls developed in rocks of the Glockner Nappe, mainly calcareous micaschists with isolated occurrences of marble and serpentinite especially at the Magnetkoepfl (Cornelius and Clar, 1935; Hoeck et al., 1994). Cleavage orientation in the predominant calcareous micaschists is similar at all rockwalls studied and dips steeply (~ 45 °) to NNE (Fig. 4). Numerous pronounced joint-sets indicate high degrees of fracturing, which is particularly evident along existing tectonic faults (e.g. at KNW) and along distinct cleavage planes (e.g. at KN, MKE). The two most prominent joint sets dip subvertical to W (J1) and steeply to SW (J2), respectively. Investigations of rock mass strength carried out in all investigated rockwalls indicate highly variable lithologic strength due to the high spatial variability in fracture density (Terweh, 2012).

Mean temperature during the study period (2011-2017) recorded at a weather station located on the Schmiedingerkees glacier (Fig. 1) was -2.0 °C. According to an empirical-statistical model of permafrost distribution for the Hohe Tauern range (Schrott et al., 2012) permafrost can be expected above 2,500 m a.s.l. on north-facing slopes and above 3,000 m a.s.l. on south-facing slopes.

Kommentiert [IH6]: Replaced by new Fig. 3 following suggestion by RC2 (R. Kenner).

RC2 (R. Kenner) wrote:
"Consider to show some 2D slope profiles including an elevation bar and aspect indication instead of table 1. Decision is up to the authors."

Kommentiert [IH7]: RC1 (A. Anders) criticised missing information on joint orientations.

2.1 Deglaciation

The Schmiedingerkees glacier has retreated considerably in recent decades and ice-~~aprons~~faces have degraded significantly in the surrounding cirque walls (Fig. 1 and Fig. 2). The oldest useable aerial photos date back to 1953 (Land Salzburg, 1953) and demonstrate a glacier area of 3.2 km². Since then the Schmiedingerkees glacier lost more than half of its size (-56 %) and ~~the glaciated area decreased to 1.4 km² (2017).~~ adjacent to the monitored rockwalls thinned by an average of 17 m (Table S8). Long-term glaciological monitoring at the nearby Stubacher Sonnblickkees glacier (located 9 km SW of the study area) shows evened mass balances between the 1950s and the early 1980s (Slupetzky and Ehgartner, 2014; Slupetzky, 2015) indicating that most of this surface change has occurred over the last 35 years.

In 2008 the first comprehensive terrain data was acquired for the Schmiedingerkees (Land Salzburg, 2008) using airborne laserscanning. The comparison with current UAV-derived terrain data demonstrates that in the period between 2008 and 2017 glacier volume decreased by 8.5~~9.8~~ million m³. Mass loss was most pronounced near the terminus, but also in the root zone, i.e. adjacent to the rockwalls in focus here~~. . Distinct ice-face degradation and glacier retreat is evident with annual surface lowering rates of around 0.5 m that exposed large, fresh bedrock surfaces (Fig. 1).~~ distinct ice-apron degradation and glacier retreat is evident. Mean ice surface lowering next to the monitored rockwalls equalled 0.7 m a^{-1} over the study period and exposed large, fresh bedrock surfaces (Fig. 1, Table S8)

~~According to a recent empirical-statistical model of permafrost distribution for the Hohe Tauern range permafrost can be expected above 2,500 m a.s.l. on north-facing slopes and above 3,000 m a.s.l. on south-facing slopes (Schrott et al., 2012). In the study area, permafrost temperatures are monitored since December 2015, in two 30 m deep boreholes located at the north- and west-face of the Kitzsteinhorn, at approximately 3,000 m a.s.l.. Bedrock temperatures below the zero annual amplitude are -1.8 °C and -1.3 °C at the north- and west-face, respectively. Maximum active layer thickness usually occurs in early September and at the north-face increased in thickness from 3.0 m in 2016, to 3.7 m in 2017, and 3.9 m in 2018.~~
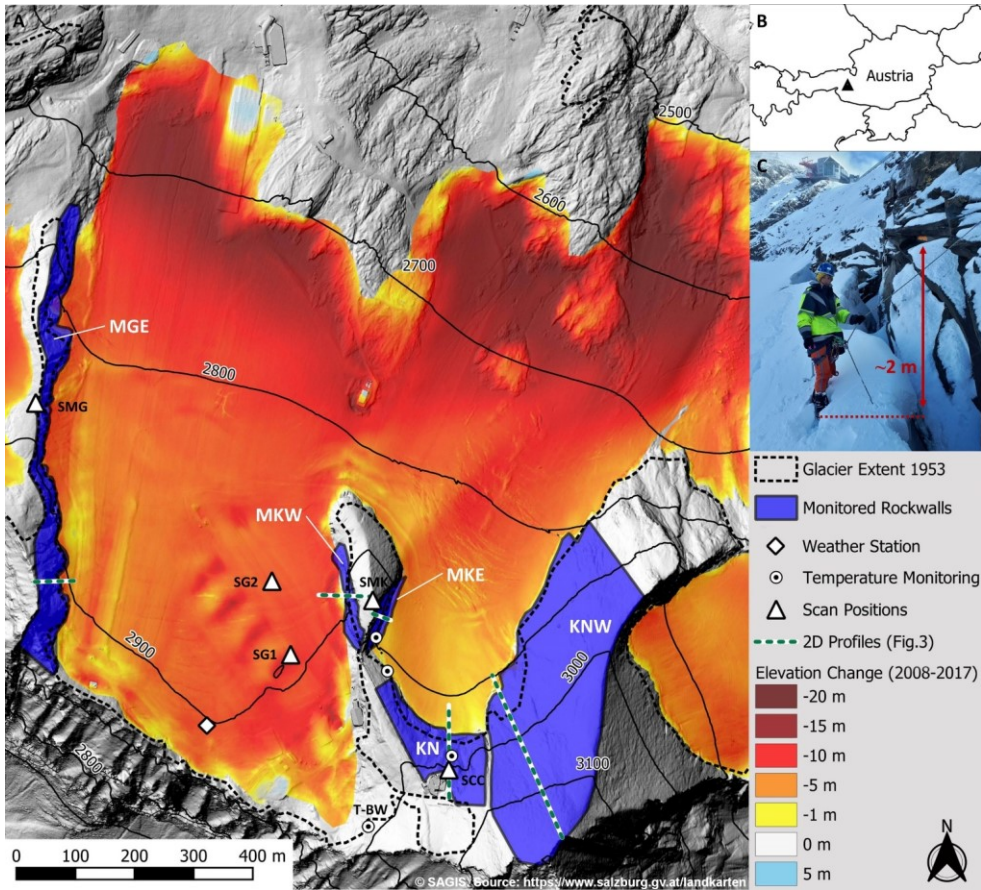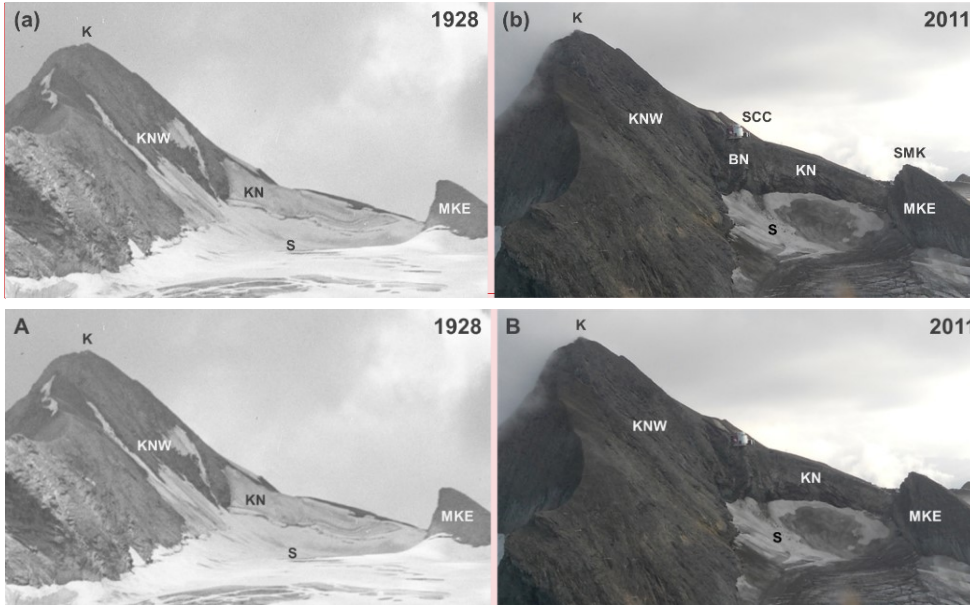
11

Figure 1A: Hillshade of study area with monitored rockwalls, scan positions, 1953 glacier extent, and elevation changes of the surface of the Schmiedingerkees glacier between 2008 and 2017. While glacial thinning is most evident near the terminus, pronounced ice surface lowering (~ 0.7~~5~~ m a⁻¹) is also observed adjacent to the monitored cirque walls. 1B~~Elevation changes were calculated based on comparison between airborne laserscanning data (2008) and UAV-derived photogrammetric data (2017). Inset (top le~~: ~~ft) shows l~~Location of study site within Austria. 1C: Glacier surface lowering 2015-2019. Orange spray marker on rockwall indicates glacier surface level on 04.09.2015 (photo: I. Hartmeyer, 09.09.2019). Abbreviations: ~~K = Kitzsteinhorn (Summit), ~~SMK = Scan Position 'Magnetkoepfl', SCC = Scan Position 'Cable Car Top Station', SG1 = Scan Position 'Glacier 1', SG2 = Scan Position 'Glacier 2', SMG = Scan Position 'Maurergrat'~~, BN = Permafrost Borehole North-Face (30 m), BW = Permafrost Borehole West-Face (30 m),~~ (for other abbreviations see text).

Figure 2: View of Kitzsteinhorn (K) (3.203 m a.s.l.) and Schmiedingerkees glacier (S) from (a) September 1928 (Photo: Stadtarchiv Salzburg, Fotosammlung Josef Kettenhuemer) and (b) September 2011 (Photo: Heinz Kugler). During the reference period the ice surface has lowered considerably while all ice-apronsfaces have completely disappeared. Much of the surface change has occurred since the 1980s. Abbreviations: BN = Borehole North-Face, SCC = Scan Position 'Cable Car Top Station', SMK = Scan Position 'Magnetkoepfl' (for other abbreviations see text).

Kommentiert [IH13]: Figure was updated (slight modification/simplification of labelling)
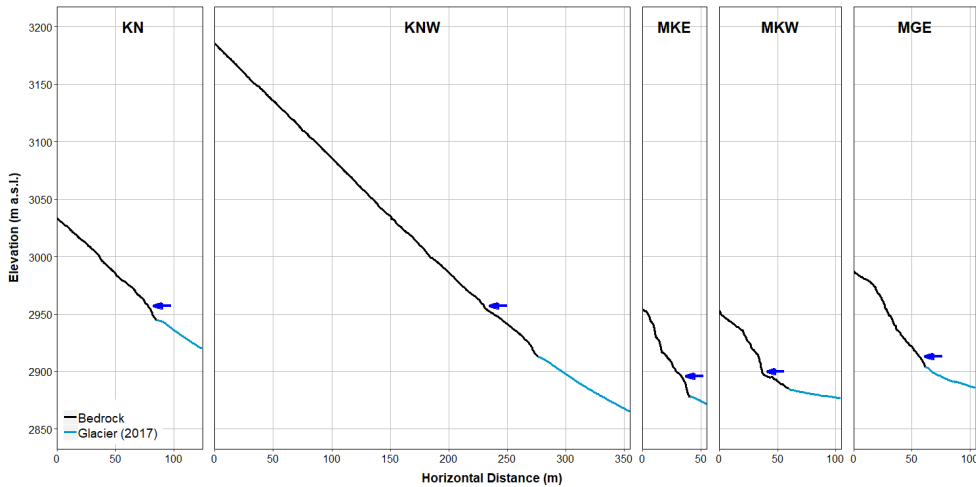
14

Figure 3: 2D slope profiles for all monitored rockwalls. Blue arrows indicate approximate level of glacier surface in 1953.
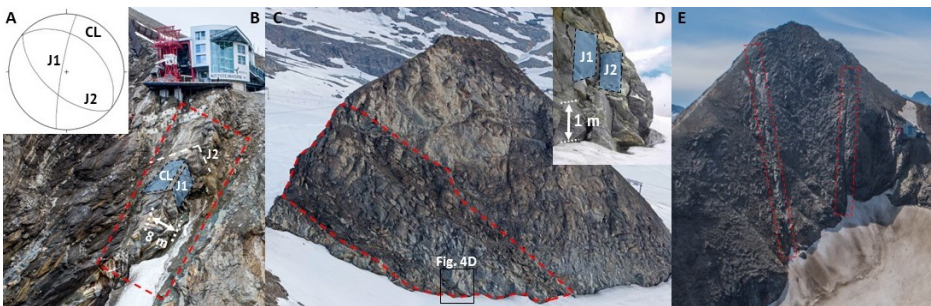
390

Figure 4: Geological structure and weakness zones at the monitored rockwalls. 4A: Cleavage (CL) of the calcareous mica-schists dips about 45° NNE. Joint sets J1 (dipping subvertical to W) and J2 (dipping steeply to SW) are approximately orthogonal to CL and predispose north-facing slopes for dip-slope failures; 4B: Highly fractured, slope-parallel escarpment at KN (photo: R. Delleske, 01.08.2018); 4C: Diagonal weakness zone following the direction of cleavage at MKE (photo: R. Delleske, 18.07.2014); 4D: Steep joint sets (J1, J2) predispose east- and west-facing areas to toppling failures (photo: A. Schober, 28.07.2010); 4E: Prominent fault lines resulting from ductile shearing at KNW (photo: R. Delleske, 27.08.2019)

15

3 Methods

3.1 Terrestrial LiDAR Monitoring

3.1.1 Data Acquisition

Terrestrial LiDAR data acquisition was performed using a Riegl LMS-Z620i laserscanner ~~(Table 1)~~. A calibrated high-resolution digital camera was mounted on the laserscanner for capturing referenced colour images. Reflectivity on bedrock

400 surfaces was excellent in the near-infrared wavelength used by the scanner, while reflectivity on fresh snow or ice was poor and returned little or no data. Reflectors were not used during data acquisition due to considerable rockfall hazard in the steep, unstable rockwalls.

First LiDAR data was acquired in July/August 2011 at all monitored rockwalls except MKW where data acquisition started in 2012. Data acquisition was restricted to the summer season (May to October). ~~Access to all scan positions required ropes and~~

405 ~~mountaineering gear, except at the Cable Car Top Station.~~ In total 78 rockwall scans were carried out from five different scan positions. Of these, 22 scans were excluded from further analyses due to snow cover. Scan position 'Maurergrat' was abandoned in 2016, as due to continued glacial thinning site access was lost. Rockwall scans were repeated several times per summer season and at least once per season towards the end of the ablation period. The last scan of all rockwalls was carried out in August 2017, except for MKW that was excluded from further analysis, as unstable blocks were cleared away earlier in

410 2017 to reduce hazards for a new lift track.

The mean object distances (i.e. distance between scanner and rockwall) differed considerably, varying between 140 m for MKW and 650 m for MGE. The acquisition resolution ranged typically between 0.01-0.02 °, ~~The~~ resulting in point cloud~~spatial~~ resolution ~~typically ranged~~ mostly between 0.1-0.3 m (see Table S3~~2~~ for full list of data acquisition parameters).

~~Table 2: Properties of the Riegl LMS-Z620i terrestrial laserscanner used for this study.~~

	~~Riegl LMS-Z620i~~
~~Range (*m*)~~	~~up to 2,000~~
~~Accuracy (*mm*)~~	~~10 (= 1σ @ 100 m)~~
~~Measurement rate (*pts/sec*)~~	~~up to 11,000~~
~~Field of view (°)~~	~~360 x 80~~
~~Wavelength~~	~~near infrared~~
~~Beam divergence (*mrad*)~~	~~0.15~~
~~Beam footprint at 100 m (*mm*)~~	~~15~~
~~Min. angular step width (°)~~	~~0.004~~
~~Referenced images~~	~~yes~~

415 **3.1.2 Data Analysis**

Airborne LiDAR datasets acquired in 2008 (Land Salzburg, 2008) were used as base data for georeferencing. Alignment of the acquired sequential point clouds was performed based on surface geometry matching within RiScanPro 1.8. First, point clouds were coarsely registered using the GPS location of the scan position and the azimuth angle of the laserscanner. Numerous techniques exist for the fine registration of point clouds, which include the Iterative-Closest-Point (ICP) algorithm

16

Kommentiert [IH16]: Deleted following suggestion by SC1 (J. Beutel).

SC1 (J. Beutel) wrote:
"The sentence about rope access is irrelevant for this study. leave it out."

Kommentiert [IH17]: Modified following suggestions by SC1 (J. Beutel).

SC1 (J. Beutel) wrote:
"Table 2: Rather than repeating the sales brochure of Riegl please specify the settings used for obtaining your data. The general specs of this instruments are known/accessible through the manufacturer to everyone."

420 (Chen and Medioni, 1992; Besl and McKay, 1992), 3D Least Squares Matching (Akca, 2007), point-to-plane approaches (Grant et al., 2012) and others. Here we used the ICP-algorithm, a popular cloud matching technique for finding the transformation between two point clouds by minimizing the square errors between corresponding entities. Consistent with previous studies on rock slope systems (Rosser et al., 2007; Abellán et al., 2011), alignment errors were ~~negligible~~ low and ~~typically~~ ranged between 1.5-3.7 ~~and 2~~ cm.

425 The two most prominent approaches to identify surface changes in successive point clouds include the identification of homologous objects to calculate displacement fields (Teza et al., 2007; Monserrat and Crosetto, 2008) and direct distance calculation (Rosser et al., 2005). Here, the latter type was applied using the M3C2 algorithm which was specifically designed for orthogonal distance measurement in complex terrain (Lague et al., 2013). ~~During the analysis, surface normal orientation is measured at a scale consistent with the local surface roughness and mean surface change is calculated along the normal~~

430 ~~direction.~~ M3C2 is frequently used to compute distances between multitemporal point clouds and has been applied in numerous studies investigating geomorphic change (e.g. Barnhart & Crosby, 2013; Cook, 2017; Esposito et al., 2017; James et al., 2017; Williams et al., 2018). Full details can be found in Lague et al. (2013). Briefly, for comparing two successive point clouds A and B, the M3C2 algorithm calculates: (i) a normal vector for any given point i of cloud A by fitting a plane to all neighbouring points NNi that are within a radius $D/2$ of i; (ii) a bounding cylinder of radius $d/2$ with the axis centred at i and oriented

435 normally. Each bounding cylinder isolates subsets of clouds A and B that are projected onto the cylinder axis; (iii) the distribution of distances along the normal is used to calculate mean positions of sub-cloud A (i_1) and sub-cloud B (i_2). The distance measured (L_{M3C2}) between i_1 and i_2 along the normal direction is stored as an attribute of i. The standard deviation of the point distribution within the bounding cylinder (a measure of local roughness) is quantified and combined with the alignment uncertainty to estimate errors and provide a parametric local confidence interval (or level of detection) for each

440 distance measurement. The confidence interval thus represents the sum of different error terms factoring in the cumulative effects of instrumental uncertainty, surface roughness related errors, and alignment uncertainty between point clouds (Hodge, 2010; Soudarissanane et al., 2011). Surface change is considered statistically significant when L_{M3C2} exceeds the local error (confidence interval) and is rejected when L_{M3C2} is smaller than the local error.

Here, a normal scale (D) of 5 m was adopted and a projection scale (d) of 1.5 m. Plausibility of M3C2 calculations was tested

445 by manually comparing each delineated area of significant surface change (rockfall source area) to computations of the Euclidean nearest-neighbour distance (direct cloud-to-cloud (C2C) calculation). To calculate rockfall volumes, the plausibility-checked results were reanalysed using the M3C2 algorithm, and (i) a fixed normal scale (D) (orthogonal to the average local terrain surface) to avoid an overlap of the bounding cylinders and thus an overestimation of rockfall volume, and (ii) using a reduced projection scale ($d = 0.25$-0.50 m) to avoid integration of unchanged terrain adjacent to the rockfall source

450 area into the distance calculation. Local grids (cell size 5 x 5 cm) containing the L_{M3C2} values of the reanalyses were then created for each rockfall source area and the rockfall volume was computed by grid cell aggregation. The distance measurement error (L_{M3C2} confidence interval) of the grid cells was aggregated for each source area to estimate the rockfall volume error at one sigma level.

Kommentiert [IH18]: Modified following suggestions by SC1 (J. Beutel) and RC2 (R. Kenner).

SC1: "*It would help if you give a short synopsis of the algorithms used (M3C2)*"

SC1 and RC1 also both criticised missing information on rockfall volume errors whose calculations is now described in more detail.

455 ~~The M3C2 algorithm has the benefits of: (i) operating directly on point clouds without the need for meshing or gridding, and thus reduces uncertainties; (ii) computing local distances between point clouds along the surface normal direction, which specifically account for terrain roughness; (iii) providing confidence intervals for all distance measurements and thus allowing to assess the significance of surface changes determined; and (iv) providing robust measures on irregular surfaces and with irregularly-spaced data which is important when comparing point clouds of variable resolutions.~~

460 ~~Volumes of detached rock were derived from the distance calculations by identifying source areas, creating local grids and by subsequent grid-cell aggregation. Uncertainties in distance data were propagated using Gaussian error propagation to compute overall uncertainties.~~ In addition to rockfall volume, following parameters were determined for each source area: mean slope aspect and gradient, elevation above glacier surface as well as maximum depth of rock detachment (determined as the maximum Euclidean nearest-neighbour distance between the pre-event and the post-event point cloud). Source areas were differentiated as bedrock (rockwall) or unconsolidated sediments (intra-rockwall sediment deposits) based on shape,

465 inclination and image colour values. Data gaps due to occlusion are considered negligible for the multitemporal rockwall analysis as obstructions, like deep gullies or protruding spurs that often hamper such analyses in heterogeneous rockwall topography, are rare and scan positions were fixed throughout (except for the final scan at MKW in 2016) for minimising potential detrimental effects from changing incidence angles. Long return periods between surveys however, increase the chance of superimposition and coalescence effects, i.e. adjacent or subsequent events are sampled as one failure only (van

470 Veen et al., 2017; Williams et al., 2018). To improve readability 'rockfall source areas' are referred to as 'rockfalls'.

3.2 Rockwall Temperature Monitoring

Bedrock temperature was monitored in two deep and four shallow boreholes. Deep borehole T-BN is located at KN about 40 m above the current glacier surface at 2,985 m a.s.l., and was drilled perpendicular to the ~ 45° terrain surface to a depth of 30 m (Fig. 5). Deep borehole T-BW (25 m) is situated at 2,975 m a.s.l. in a W-facing rock slope (~ 40°) not monitored with

475 terrestrial LiDAR (Fig. 1). Borehole temperature was recorded at eleven (T-BW) and twelve (T-BN) different depths with an accuracy of ± 0.03 °C (Platinum Resistance Temperature Detector L220, 1/10 B, Heraeus Sensor Technology).

A vertical transect consisting of three shallow boreholes (0.8 m deep) was established in a NE-facing section at KN in September 2015 to investigate bedrock temperatures inside the Randkluft (Fig. 5A). The three boreholes are situated (i) at the Randkluft aperture (at glacier surface level) (T-RK1, Fig. 5B and 5E), (ii) 7 m below the glacier surface (T-RK2, Fig. 5C), and

480 (iii) 14 m below the glacier surface (T-RK3, Fig. 5D). Another shallow borehole (0.8 m deep) is located around 5 m above the glacier surface in a ESE-facing section at MKE (T-MKE, Fig. 5A). Temperature in all shallow boreholes is measured with wireless miniature data loggers with an accuracy of ± 0.1 °C (Geoprecision M-Log5W-Rock).

**Kommentiert [IH19]:** Deleted following suggestions by SC1 (J. Beutel).

SC1 (J. Beutel) originally wrote:
"It would help if you give a short synopsis of the algorithms used (M3C2) and not only list benefits"

Kommentiert [IH20]: SC1 (J. Beutel) criticised that it was unclear how rockfall volume errors are calculated. Explanation of rockfall volume error calculation was therefore expanded (see immediately above).

Kommentiert [IH21]: Modified following suggestion by RC2 (R. Kenner):

RC2 (R. Kenner) wrote:
"How did you considered shadow effects, i.e. data gaps?"

Kommentiert [IH22]: Subchapter added following suggestions by RC1 (A. Anders), SC1 (J. Beutel) and RC2 (R. Kenner) who all asked for a more thorough thermal characterisation of the studied rockwalls.
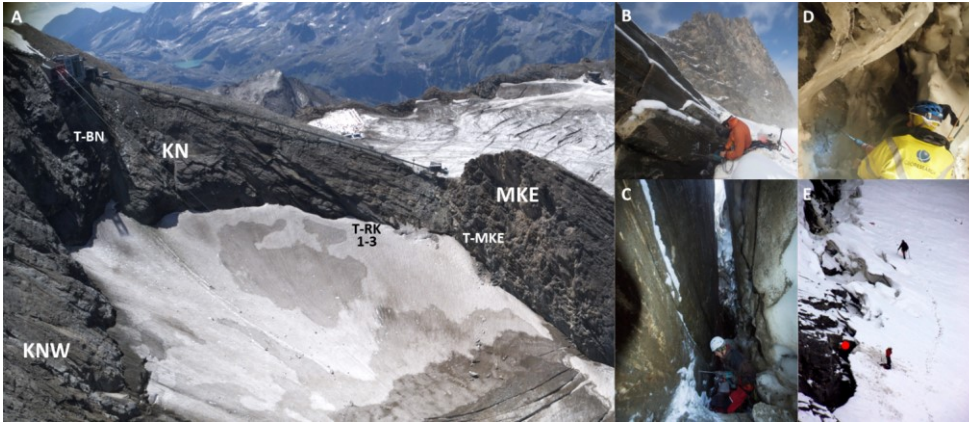
Figure 5: Deep and shallow borehole temperature monitoring at Kitzsteinhorn. A: Overview image (photo: R. Delleske, 24.08.2017); B: Measurement site at the Randkluft aperture (T-RK1) (photo: I. Hartmeyer: 04.09.2015); C: Measurement site inside Randkluft, 7 m below glacier surface (photo: R. Delleske, 04.09.2015); D: Measurement site inside Randkluft, 14 m below glacier surface (photo: M. Dörfler, 21.09.2018); E: Close-up of the Randkluft; red dot indicates position of T-RK1 (photo: F. Miesen, 04.09.2016).
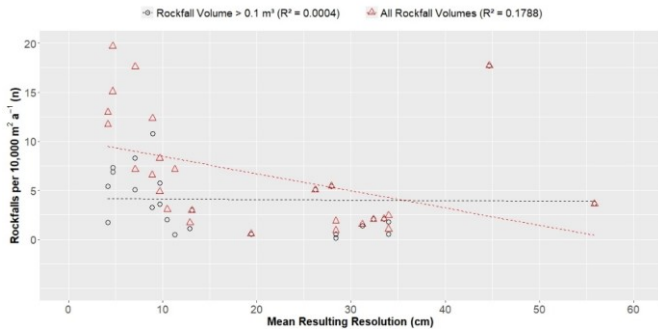
4 Results

4.1 LiDAR Data Resolution~~Quality~~

~~To investigate the level of confidence that can be given to the scan results, instrumental and referencing uncertainties were quantified, assumed to be normally distributed, propagated using Gaussian error law and are given at one sigma level.~~ ~~The mean relative error associated with rockfall volumes is 0.1 %. Relative errors are smaller for large rockfall volumes than for small volumes closer to detection limits. Uncertainty for rockfalls smaller than 1 m³ is 0.8 %, while for large rockfalls over 100 m³ relative errors drop to 0.01 % (see Table S3).~~ Data resolution (point density) plays a key role for defining smallest distinguishable detail in point clouds (Hodge, 2010). As a result, more low-magnitude rockfalls will be detected in high-resolution scans compared to low-resolution scans, which introduces issues when rockfall numbers based on scans of differing data resolution are to be compared. ~~The resulting resolution varies between different scans and theoretically leads to the detection of a larger number of small rockfalls in high-resolution scans than in low-resolution scans. This correlation is problematic when scans with different resolutions are compared.~~ To constrain ~~this~~ the influence of data resolution, the mean resulting resolution is compared to the normali~~z~~sed number of rockfalls detected (i.e. the number of rockfalls per 10,000 m² per year) in Fig. 6. A~~, which suggests a~~ weak positive correlation (R² = 0.18) ~~(Fig. 3).~~ ~~can be observed and~~ ~~F~~for rockfalls larger than 0.1 m³ the number of rockfalls is independent of resolution. All~~and~~ further analyses were~~was~~ limited to ~~this size class~~rockfall volumes above this volume threshold.~~.~~ ~~This level of detection~~ Compared to other studies, the minimum usable

19

<div style="text-align: right">Kommentiert [IH23]: This is now described in more detail in Sect. 3.1.2</div>

<div style="text-align: right">Kommentiert [IH24]: Transferred to Sect. 4.2</div>

505 volume of 0.1 m³ derived here is higher ~~is less precise~~ than values specified in ~~related~~ LiDAR-based change detection surveys using~~relying on~~ shorter object distances and higher point densities (e.g. Rosser et al., 2007; Williams et al., 2018) but is~~is~~ in good agreement with similar monitoring campaigns carried out in high-alpine settings (e.g. Strunden et al., 2015).

Figure 6~~3~~: **Detected number of rockfalls per 10,000 m² a⁻¹ plotted against ~~scan~~ the mean resulting resolution of the performed**
510 **laserscans. Varying resolutions between acquired scans do not bias the detection of rockfalls larger than 0.1 m³. Dashed lines represent the regression lines of both distributions.**

4.2 ~~Inventory of Mass Movements~~Rockfall Inventory

During the six-year monitoring period (2011-2017) 632 rockfalls were registered with a total volume of 2,564.3 ± ~~1.5~~141.9
m³. When omitting rockfalls below the chosen~~-~~ threshold of 0.1 m³ (Sect. 4.1), the total number drops to 374, while the overall
515 volume is reduced only marginally to 2,551.4 ± ~~1.3~~136.8 m³ (Table 3~~1~~). The mean relative error associated with the rockfall volumes is 5.5 % and similar to other high-alpine LiDAR studies which also found single-digit relative errors (Kenner et al., 2011; Strunden et al., 2015). Relative errors are smaller for large rockfall volumes than for small volumes. Uncertainty for rockfalls smaller than 1 m³ is 29.2 %, while for large rockfalls over 100 m³ relative errors drop to 2.2 % due to reduced cumulative effects of instrumental, surface and alignment errors on larger geometries (Hodge, 2010) (see Table S4).

520 Large rockfalls over 100 m³ are rare (n = 5) but account for more than two thirds (68.5 %) of the total volume. The largest registered rockfall has a volume of 879.4 ± 6.3 m³, the volumes of the three next largest rockfalls range between 200-300 m³. With increasing volume an exponential decrease in number of rockfalls can be observed. Small rockfalls below 1 m³ represent 80 % of the total number but account for only 3.7 % of the overall rockfall volume (see companion study Hartmeyer et al., 2020) for detailed discussion of magnitude-frequency distributions).

525

Table 1~~3~~: **Absolute and normalised rockfall N~~n~~umbers (n) and volume~~s~~ (m³) ~~of registered rockfalls~~ (> 0.1 m³). Normalised rockfall number (volume) refers to rockfall number (volume) per 10,000 m² per year.**

			TOTAL	KN	KNW	MKE	MKW	MGE
0.1 - 1 m³	Number (n)	Abs.	299	83	150	15	8	43

20

		Norm.	2.15	5.89	1.87	2.25	3.20	1.19
	Volume (m³)	Abs.	94.7	24.5	45.9	6.7	2.8	14.8
		Norm.	0.7	1.7	0.6	1.0	1.1	0.4
1 - 10 m³	Number (n)	Abs.	50	13	21	4	5	7
		Norm.	0.37	0.92	0.26	0.60	2.00	0.19
	Volume (m³)	Abs.	151.8	48.3	65.9	12.6	10.7	14.4
		Norm.	1.1	3.4	0.8	1.9	4.3	0.4
10 - 100 m³	Number (n)	Abs.	20	5	7	3	2	3
		Norm.	0.15	0.35	0.09	0.45	0.80	0.08
	Volume (m³)	Abs.	547.8	104.6	156.7	54.0	136.2	96.4
		Norm.	4.4	7.4	2.0	8.1	54.4	2.7
100 - 1,000 m³	Number (n)	Abs.	5	3	1	1	-	-
		Norm.	0.04	0.21	0.01	0.15	-	-
	Volume (m³)	Abs.	1,757.0	1,278.0	272.7	206.3	-	-
		Norm.	12.5	90.7	3.4	30.9	-	-
All Rockfalls	Number (n)	Abs.	374	104	179	23	15	53
		Norm.	2.71	7.38	2.24	3.45	6.00	1.46
	Volume (m³)	Abs.	2,551.4	1,455.4	541.2	279.6	149.7	125.5
		Norm.	18.7	103.3	6.8	41.9	59.9	3.5

		TOTAL	KN	KNW	MKE	MKW	MGE
0.1 - 1 m³	Number (n)	299	83	150	15	8	43
	Volume (m³)	94.7	24.5	45.9	6.7	2.8	14.8
1 - 10 m³	Number (n)	50	13	21	4	5	7
	Volume (m³)	151.8	48.3	65.9	12.6	10.7	14.4
10 - 100 m³	Number (n)	20	5	7	3	2	3
	Volume (m³)	547.8	104.6	156.7	54.0	136.2	96.4
100 - 1,000 m³	Number (n)	5	3	1	1	-	-
	Volume (m³)	1757.0	1278.0	272.7	206.3	-	-
All Rockfalls	Number (n)	374	104	179	23	15	53
	Volume (m³)	2,551.4	1,455.4	541.2	279.6	149.7	125.5

Large rockfalls over 100 m³ are rare (n = 5) but account for more than two thirds (68.5 %) of the total volume. The largest registered rockfall has a volume of 879.4 m³, the volumes of the three next largest rockfalls range between 200 - 300 m³. With increasing volume an exponential decrease in number of rockfalls can be observed. Small rockfalls below 1 m³ represent 80 % of the total number but account for only 3.7 % of the overall rockfall volume (see companion study (Hartmeyer et al., submitted) for detailed discussion of magnitude-frequency distributions).

Frontal ~~photographs~~ views of the monitored rockwalls with indicated rockfall source areas are provided in Fig. ~~7~~4 and in the supplement (Fig. S1) and show a concentration of rockfalls along heavily fractured, structural weaknesses. Highest rockfall activity was observed at KN, which has developed parallel to the cleavage dip (~ 45° NNE) and is dissected by a highly fractured, slope parallel escarpment running from the cable car summit station to the current glacier margin (Fig. 4B). No rockfall activity was registered in the upper half of the escarpment, whereas in the lower, glacier-proximal half high activity was observed during the entire monitoring period (Fig. 7A). Three out of the five largest rockfalls in the entire study area detached from this area forming large cubic to rhomboidal blocks of up to 5 m length. The largest of the events occurred on August 18th, 2012 at around 15:00 and was visually and acoustically observed by the cable car staff and by tourist visitors.

Immediately adjacent to the glacier several joint-bordered rock bodies were detached resulting in a blockslide (Fig. 8A and B). After detachment, blocks were either retained by the glacier immediately below the source area, or slid over the glacier surface for more than 200 m carving distinct chutes into the firn covering the glacier (Fig. 8G). The lowest part of the detached rock fragment was covered by snow/firn (Fig. 8A) and was not imaged on the laserscan predating the event (August 2011). The calculated rockfall volume (879.4 ± 6.3 m³) only refers to relief visible above the glacier surface and thus represents a slight underestimate of the true volume.

Rockfall activity at the steep MKE (mean slope 71°) is largely restricted to a zone of highly fractured micaschists that runs diagonally through the rockwall following the cleavage direction (Fig. 4C). Instability within this weakness zone is highest in the immediate vicinity of the glacier surface where on August 27th, 2011 around 23:00 a 206.3 ± 11.6 m³ rockfall event occurred (Fig. 7B and 8D). The event was registered acoustically by the cable car staff and represents the fourth largest rockfall recorded during the six-year study period. The lower edge of the source area was at glacier surface level, detached blocks were either deposited immediately at the glacier margin or transported towards the glacier's centre for a maximum of 80 m (Fig. 8D). Due to the steepness of the dominant joint sets (J1, J2) the rockfall probably occurred as toppling failure.

At the other side of the Magnetkoepfl (MKW) a steep scarp was created in the centre of the rockwall by several rockfalls that occurred in the decades prior to the start of the measurements (personal communication by cable car staff) (Fig. 7C and 8F). The rockfall scarp remained a prominent source area for rockfall during the monitoring period, including two events > 50 m³ (79.3 ± 7.5 m³, 57.0 ± 4.1 m³) that detached immediately above the talus cone created by past rockfall activity.

At KNW rockfall activity mainly concentrated along a prominent fault across the entire rockwall (Fig. 7D, 8C and 4E), which included the second largest rockfall (272.7 ± 11.4 m³) observed during the monitoring period. Its rockfall source area is located 97 m above the glacier surface and may coincide with the LGM trim line. The exact date of the rockfall is unknown, photographs taken on August 26th, 2016 demonstrate fresh deposits at the glacier surface (Fig. 8C), pointing to an event date in the preceding days or weeks.

Among the rockwalls investigated rockfall activity was lowest at MGE (see normalised numbers/volumes at Tab. 1). High activity was restricted to an incised couloir at the south end of the rockwall where a 56.2 ± 4.1 m³ rockfall occurred between August 21st and September 11th, 2012. The source area was located 10 m above the glacier surface, detached blocks slid onto the glacier surface and were deposited several tens of metres from the rockwall (Fig. 7E and 8E).

The source areas and rockfall volumes (> 0.1 m³) indicate that pre-existing weaknesses exert a strong control on rockfall occurrence. Concentration of rockfalls around fracture systems is particularly evident at KN (along cleavage planes) and KNW (along a prominent fault across the entire rockwall). The highest number of rockfalls was found at the largest rockwall KNW (n = 179). Lowest rockfall numbers were recorded at the smallest rockwalls at Magnetkoepfl (MKE, MKW) (Table 1). By far the highest total rockfall volume ($1,455.4 \pm 0.2$ m³) was found at KN despite its relatively small size. Three of the five largest rockfalls occurred here. The second highest total volume was detected at KNW (541.2 ± 0.6 m³), while the lowest volume was recorded at MGE (125.5 ± 0.2 m³).
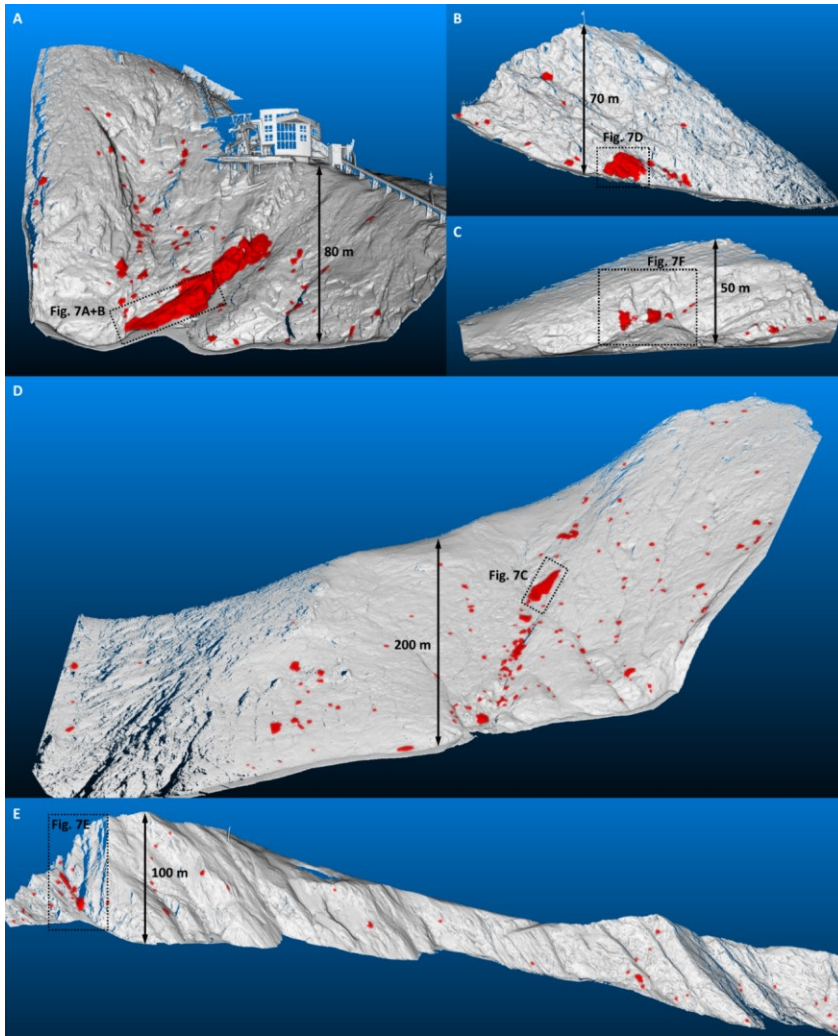
22

Figure 7: Frontal views of monitored rockwalls. Rockfall source areas identified during the six-year monitoring period are indicated in red. 7A: Kitzsteinhorn north-face (KN); 7B: Magnetkoepfl east-face (MKE); 7C: Magnetkoepfl west-face (MKW); 7D: Kitzsteinhorn northwest-face (KNW); 7E: Maurergrat east-face (MGE). Displayed topography and glacier level were taken from the most recent LiDAR survey (i.e. from 2017 for all rockwalls except MKW).
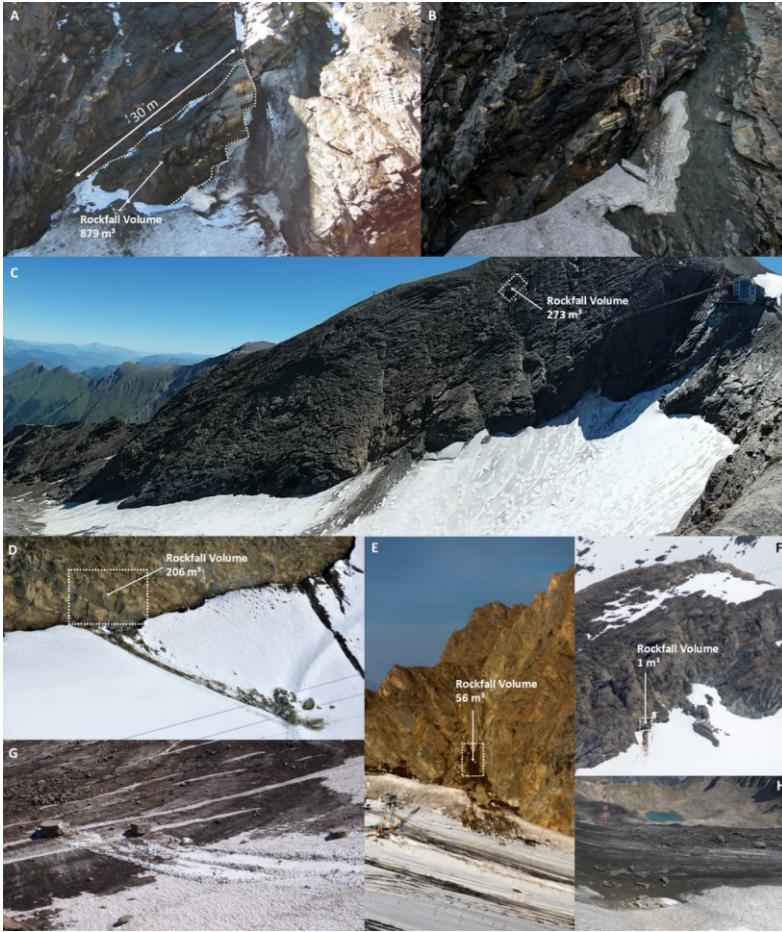
Figure 8: Documentation of rockfall events for all monitored rockwalls. 8A: Pre-event topography of the largest rockfall registered in the study period at KN (879.4 ± 6.3 m³), the remnant of an ice-apron is visible directly right of the source area (photo: M. Keuschnig, 17.08.2011); 8B: Post-event topography of the event (photo: R. Delleske, 28.08.2019); 8C: Fresh deposits on the glacier surface after 272.7 ± 11.4 m³ (second largest event recorded) of rock detached 97 m above the glacier at KNW (photo: I. Hartmeyer, 26.08.2016); 8D: 206.3 ± 11.6 m³ rockfall at the foot of MKE (photo: I. Hartmeyer, 05.11.2011); 8E: Fresh rockfall deposits below a couloir at south end of MGE after a 56.2 ± 4.1 m³ rockfall (photo: R. Delleske, 12.09.2012); 8F: Small rockfall event (1.3 ± 0.3 m³) at MKW (photo: R. Delleske, 12.09.2012); 8G: Cubic blocks deposited on glacier after event described in 7A (photo: I. Hartmeyer, 17.08.2012); 8H: Extensive cover of rockfall deposits on the central part of the Schmiedingerkees glacier (photo: I. Hartmeyer, 18.09.2018).

580

585

24

4.3 Other Mass Movements

In addition to rockfalls, 113 source areas ~~of slide-, creep- or debris-flow-like mass movements~~ were identified in unconsolidated sediments. The total volume of these mass movements is 292.0 ± 72.3~~0.4~~ m³. Nine mass movements larger than 10 m³ were identified and account for 56.2 % of the total volume. The size distribution follows the pattern of rockfall volume distribution where smaller mass movements are frequent but represented only a small part of the overall volume and show an exponential decrease in number with increasing volume (Table S5~~4~~). These types of mass movement were almost fully limited to KNW and KN. The two rockwalls are the least steep and permit accumulation of thin sediment veneers on intra-rockwall couloirs and ledges. Together, KNW and KN display 90.3 % of the total number and 99.3 % of the total volume of all loose sediment movements.
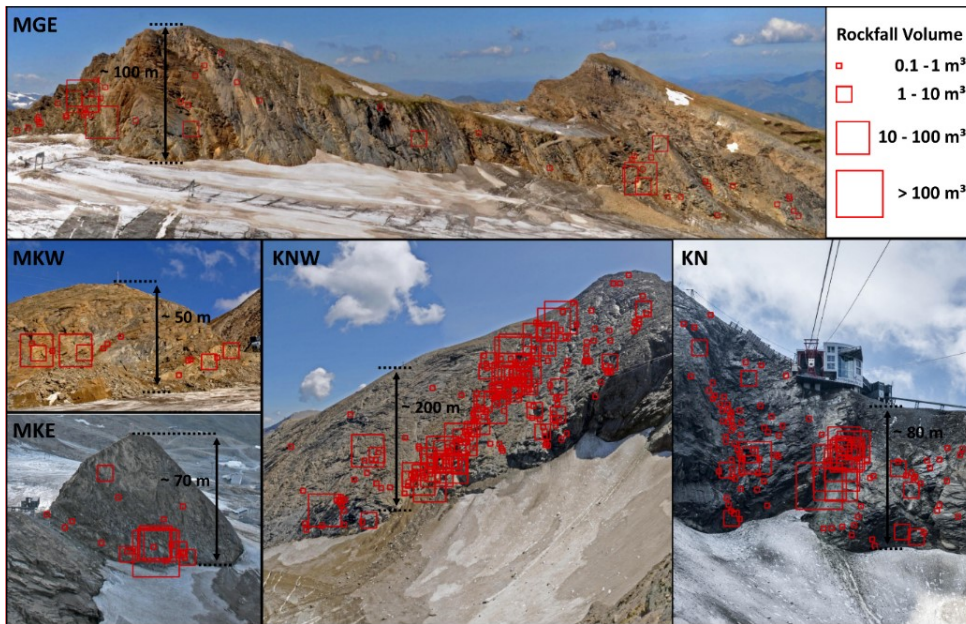
~~Figure 4: Rockfall source areas and volumes for all five monitored rockwalls. A clear linear distribution along major joint intersections is evident at all rockwalls and is particularly apparent at KNW (Kitzsteinhorn northwest-face) and KN (Kitzsteinhorn north-face) (Photos: Robert Delleske).~~

Further mass losses identified relate to ice-apron~~face~~ degradation in ~~four~~ a well-shaded location~~s~~ at the lower part of KN adjacent to the glacier surface (Fig. 8A and B). The overall ice loss from 2011-2017 was 575.9 ± 73.9~~0.04~~ m³. The single

Kommentiert [IH29]: Modified following suggestion by RC2 (R. Kenner).

RC2 (R. Kenner) wrote:
"How can you determine the volume of a slowly creeping mass?"

Kommentiert [IH30]: Shifted to supplement. (Replaced by new Fig. 7 and 8).

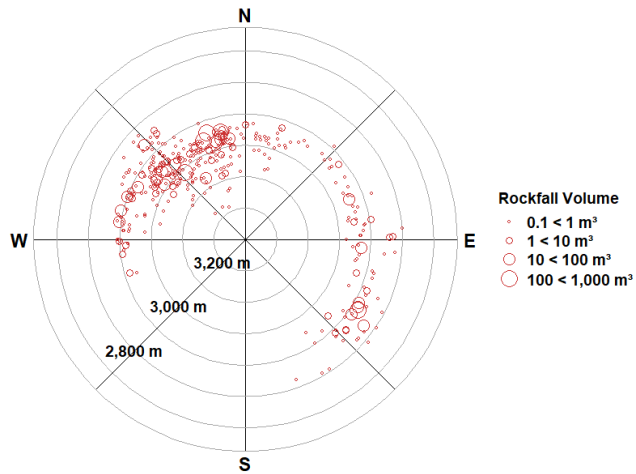**Kommentiert [IH31]:** Reference to figure added following suggestion by RC2 (R. Kenner).

RC2 (R. Kenner) wrote:
"not visible at the photo?"

biggest recorded ice loss was 424.1 ± 60.7 m³ between August 2012 and August 2015 (no data acquisition in 2013 and 2014 due to persistent snow cover), followed by mass losses of 66.8 ± 4.6 m³ and 51.4 ± 4.8 m³ between August 2016 and August 2017, and a mass loss of 33.6 ± 3.8 m³ between August 2015 and August 2016. The two mass losses recorded between 2016 and 2017 are underestimated as late snow cover during the second scan obscured the rockwall.

610 **4.3~~4~~ Directional ~~Spatial~~ Rockfall Distribution**

Directional analysis of rockwall surface area demonstrates highest shares in the NW-sector (45 %) due to the dominant influence of KNW, followed by E- and N-facing areas (17 % each). S-oriented source areas are largely missing due to the absence of significant S-faces in the study area (Fig. 9A). The bulk of the registered rockfalls originated in N- and NW-oriented rockwall sections between 2,900 and 3,100 m a.s.l.~~, mostly due to the dominant influence of KN and KNW which are both~~

615 ~~dissected by pronounced weakness zones~~. E~~ast~~-facing rockfall source areas between 2,800 and 3,000 m a.s.l. represent another distinct azimuth cluster (Fig. ~~5~~9B). Normalised rockfall volume (i.e. rockfall volume per 10,000 m² per year) is significantly elevated in the N-, W- and SE-sector and low for all other slope aspect sectors (Fig. 9C). Normalised rockfall numbers (i.e. rockfall number per 10,000 m² per year) peak in the same sectors as normalised rockfall volume (except for the S-sector, which however is represented by just a single rockfall) (Fig. 9D). High (normalised) activity in N-, W- and SE-sectors most likely

620 reflects the dominant discontinuity orientations at the study site which promote the detachment of cubic to rhomboidal detachments in N-facing areas and failures along steep joint systems in W- and SE-facing areas (Fig. 4).

Kommentiert [IH32]: This subchapter was added following suggestions by RC1 (A. Anders) and SC1 (J. Beutel) to provide more information on the directional/sectoral distribution of rockfalls.

26

625
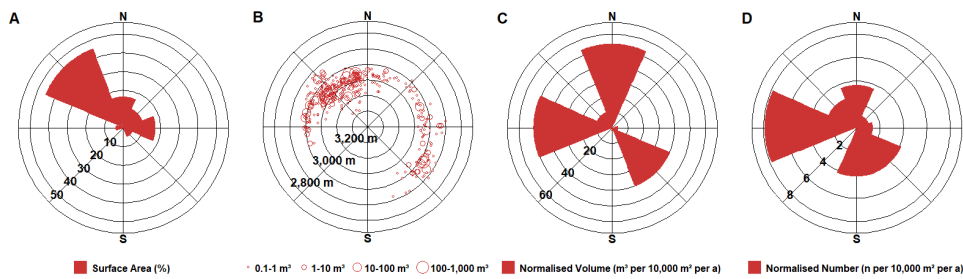
Figure 9A: Sectoral distribution of surface area. 9B: Slope azimuth angle and elevation above sea level for all rockfalls. 9C: Normalised rockfall volume by sector (m³ 10,000 m^{-2} a^{-1}). 9D: Normalised rockfall number by sector (n 10,000 m^{-2} a^{-1}).

630

Figure 5: Slope azimuth angle and elevation above sea level for all rockfalls (> 0.1 m³). Most rockfalls originated in N- and NW-oriented rockwall sections reflecting the dominant influence of KN (Kitzsteinhorn north-face) and KNW (Kitzsteinhorn northwest-face).

4.5 Altitudinal Rockfall Distribution

To further explore rockfall distribution with elevation, we classified the investigated surfaces into vertical 50 m bins. Total rockwall surface area is almost normally distributed and shows the largest share between 2,900-2,950 m a.s.l. (~ 65,000 m²; 27.0 % of total surface area) (Fig. 610a and Table S65). Normalisзed and absolute rockfall volumes peak in the same elevation class. Over 37 m³ per 10,000 m² a⁻¹ originated between 2,900-2,950 m a.s.l. (Fig. 610b), which is equivalent to more than half (54.4 %) of the total rockfall volume (Table S65).

The normalisзed number of rockfalls is highest between 2,950-3,000 m a.s.l. (4.6 rockfalls per 10,000 m² a⁻¹) and declines significantly . Wwith increasing/decreasing elevation, ~~normalized rockfall numbers decline significantly, similar to the altitudinal distribution of surface area~~ (Fig. 610c). Absolute rockfall numbers peak between 2,900-2,950 m a.s.l. and 2,950-3,000 m a.s.l., where approximately two thirds (63.8 %) of the detected rockfalls originate (Table S65).

To detail the vertical distribution of rockfall source areas, the elevation differences between rockfall source areas and local glacier surface are calculated and grouped into 10 m bins (Fig. 711a and Table S21). Immediately above the glacier surface (0-10 m) rockfall volumes are by far the highest (75.6 m³ per 10,000 m² a⁻¹) (Fig. 711b). 60 % of the total rockfall volume detached from this segment, which constitutes only 15 % of the total rockwall surface area. With increasing distance from the glacier surface, a sharp decrease in rockfall volume can be observed. In the next higher segment (10-20 m), normalisзed rockfall volume slightly exceeds 20 m³ per 10,000 m² a⁻¹, while in all other height classes rates remain below 10 m³ per 10,000 m² a⁻¹. Only in two segments (90-100 m, 170-180 m), this pattern is masked by the presence of comparatively large, singular rockfalls.
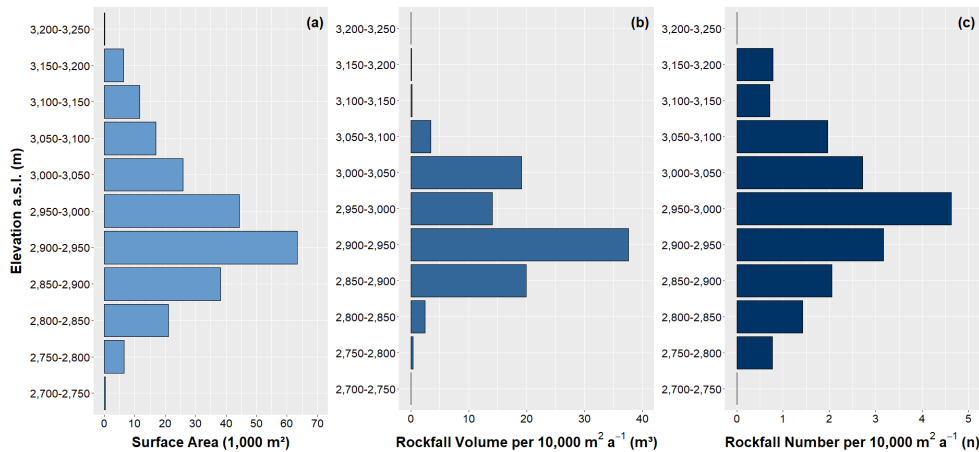
<div style="color:gray">**Kommentiert [IH34]:** Modified following correction by RC2 (R. Kenner).

RC2 (R. Kenner) wrote:
"Is this of relevance if the values are normalized by area?"</div>

Figure 106: (a) Rockwall surface area, (b) normalisзed rockfall volume and (c) the normalisзed number of rockfalls, grouped by elevation above sea level. Between 2,900 and 2,950 m a.s.l. a distinct peak in rockfall volume is observed.

Analysed individually, a positive correlation between rockfall volume and proximity to glacier surface occurs for all rockwalls except KNW. The vast majority of the rockfall volume is detected within 10 m of the glacier surface at MGE (73 %), KN (79 %) and MKE (98 %). Considering the first 20 m above glacier surface the volume percentages exceed 90 % for all three rockwalls.

660 At MKW rockfall volumes are small in the lowest segment (3 %) and 96 % of the ~~total~~ rockfall volume occur in the segment above (10-20 m). Here, ~~a rockfall event from the early 2000s~~rockfall activity in decades prior to the start of the monitoring, created a steep scarp around 15 m above the current glacier surface. The rockfall deposits, likely several thousand cubic meters of rock, accumulated at the foot of MKW and constituted a talus cone that decoupled parts of the rockwall from the glacier. ~~The rockfall scarp remained a prominent source area for rockfall during the monitoring period~~Numerous rockfalls detached
665 from this scarp during the study period, indicating continued stress release after the ~~initial~~ preceding events. ~~Rockfall from this scarp was the main reason why this rockwall displays a differing pattern and maximum retreat rate does not occur within the first ten vertical meters above glacier surface.~~

As mentioned no pronounced glacial proximity pattern was found for KNW, where only 12 % of the rockfall volume detached within the first 10 m. Here, a significant 272.7 ± 11.4~~0.03~~ m³ rockfall occurred in summer 2016 (Sect. 4.2) which constituted
670 around half of the total rockfall volume at this site. ~~Its rockfall source area is located 97 m above the glacier surface and may coincide with the LGM trim line.~~ Still, after excluding this event, only a rather weak proximity pattern is observed (23 % of the volume within the lowest 10 m) clearly deviating from the patterns observed at the other four rockwalls.

Analysis of rockfall numbers confirms the glacial proximity pattern even though the correlation is much less pronounced than for the elevation volume distribution. Highest normali~~z~~sed rockfall numbers (3.9 rockfalls per 10,000 m² a^{-1}) are once again
675 found in the lowest segment (0-10 m) (Fig. 7c). The mean value for all higher segments (i.e. 10-260 m) equals 2.5 rockfalls per 10,000 m² a^{-1} with significant variations between the different height classes. Overall 21 % of all rockfalls (78 of 374) occurred in the first 10 m above the glacier surface – a distinct contrast to the dominance of rockfall volumes in that segment. Comparing rockfall numbers across the rockwalls yields diverse results: At KN particularly high rockfall numbers are found between 30 and 50 m above the glacier. KNW shows a more uniform pattern with a rather balanced distribution over the first
680 100 m and a slight decrease at higher elevations. At MKE, rockfall is restricted to the immediate adjacency to the glacier and above the 0-10m-segment only minimal rockfall activity is observed. At MKW and MGE, most rockfalls occurred within 20 m of the glacier surface (~ 70 % and 90 %, respectively).

Kommentiert [IH35]: Modified following question by RC2 (R. Kenner).

RC2 (R. Kenner) wrote:
"this is ambigious. total rock fall volume or mean rock fall volume?"

Kommentiert [IH36]: Slightly modified for consistency with new passages in Sect. 4.2.

Kommentiert [IH37]: Modified following question by RC2 (R. Kenner):

RC2 (R. Kenner) wrote:
"This is impossible when looking at figure 7c?"

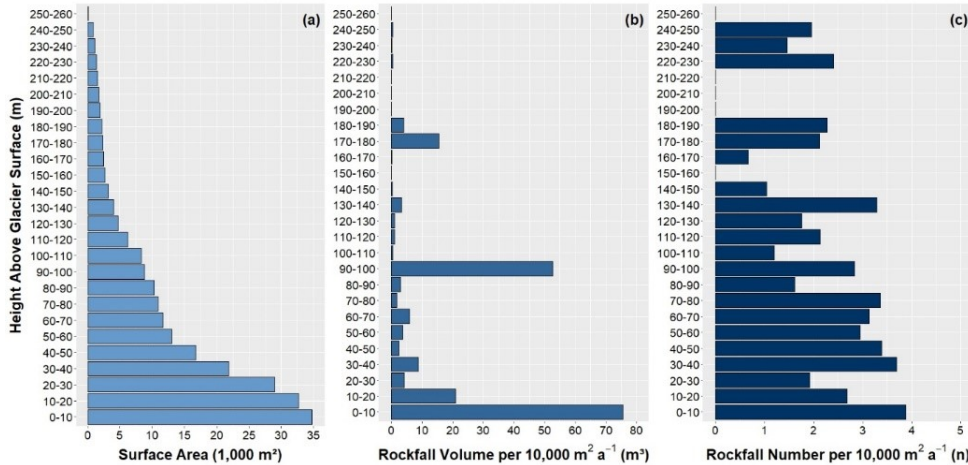Explanation: Fig. 7c (now Fig. 11c) gives the normalised rockfall number.

Figure 11: (a) Rockwall surface area, (b) normalised rockfall volume and (c) the normalised number of rockfalls, classified by elevation above glacier surface. Areas exposed by recent glacier retreat are heavily susceptible to rockfall, during the observation period (2011-2017) 60 % of the total rockfall volume detached within 10 m of the current glacier surface.

The observed distribution of rockfall magnitudes and frequencies is described by a distinct negative power function over four orders of magnitude (Fig. 12). To test the statistical robustness of the discovered differences between glacier-proximal (< 10 m above glacier) and glacier-distal (> 10 m above glacier) rockfall activity the goodness of fit was analysed using a bootstrapping approach (full details are given in Hartmeyer et al., 2020). In the analysis 20 % of the rockfalls were randomly removed and the data set was resampled 100,000 times to assess the sensitivity of the power-law-exponent b, which represents a frequently used variable to characterise spatiotemporal rockfall variation (e.g. Dussauge-Peisser et al., 2002; Barlow et al., 2012). Results demonstrate robust power law exponent b estimates of $0.51^{+0.07}_{-0.05}$ for the proximal and $0.69^{+0.04}_{-0.03}$ for the distal datasets at 95 % confidence level.

To selectively examine the statistical sensitivity to individual rare events, the power-law-fits were recalculated after omitting the five largest rockfalls (volumes > 100 m³). Power law exponents for proximal rockfalls ($0.59^{+0.07}_{-0.05}$) and distal rockfalls ($0.71^{+0.04}_{-0.03}$) only slightly increase and show the significance of the differences observed between proximal and distal areas. Normalised rockfall volume in proximal areas (11.7 m³ per 10,000 m² a⁻¹) was 2.6 times higher than in distal areas (5.2 m³ per 10,000 m² a⁻¹) in the reduced data set (volumes > 100 m³ omitted).

Kommentiert [IH38]: Modified following suggestion by RC2 (R. Kenner)

RC2 (R. Kenner) wrote
"You did a good job in estimating the accuracy of your measurements. However, I miss something similar for the statistics. Some of the statistical analysis are based on very small sample sizes or are strongly influenced by single events. I wonder if all this is significant and would appreciate something like a sensitivity analysis."
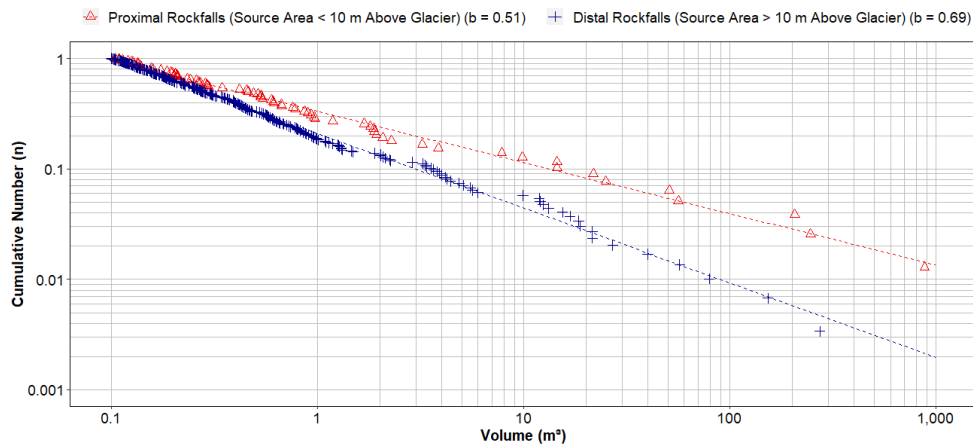
Figure 12: Magnitude-frequency distributions for glacier-proximal rockfalls and glacier-distal rockfalls. Proximal rockfalls (b = 0.51) are fitted by a significantly flatter regression line than distal rockfalls (b = 0.69) indicating an increased occurrence of large events in recently deglaciated areas.

4.4~~6~~ Rockfall Failure Depths

Among the 374 rockfalls identified~~To compare rockfall patterns to depth of permafrost thaw,~~, depth of failure ~~was analysed which~~ ranges between 0.17 and 6.45 m. Near-surface failures ~~are~~ dominan~~te~~t as 69 % of all rockfalls failed within the top 0.5 m and another 22 % ~~had failure~~in depths between 0.5 and 1 m. Eleven rockfalls with failure depths of more than 2.0 m were recorded (2.9 %) and only five rockfalls failed in depths larger than 3.0 m (1.3 %) (Fig. ~~8~~13, Table S~~7~~6). Classification of rockfall failure depth by slope aspect demonstrates an increased occurrence of relatively deep failures (> 1 m, > 2 m) in W-, SE-, and N-facing areas (Table 2). This pattern is consistent with dominant local discontinuities which predispose N-facing rockwall sections to thick dip-slope failures along the NNE-dipping cleavage, as well as W- and SE-facing sections to large (toppling) failures along the steep joint sets J1 and J2 (Fig. 4).

> **Kommentiert [IH39]:** Modified following suggestion by RC1 (A. Anders).
>
> RC1 (A. Anders) wrote:
> *"Is there a difference in the thickness of the rockfalls with orientation (or a pattern related to location)?"*
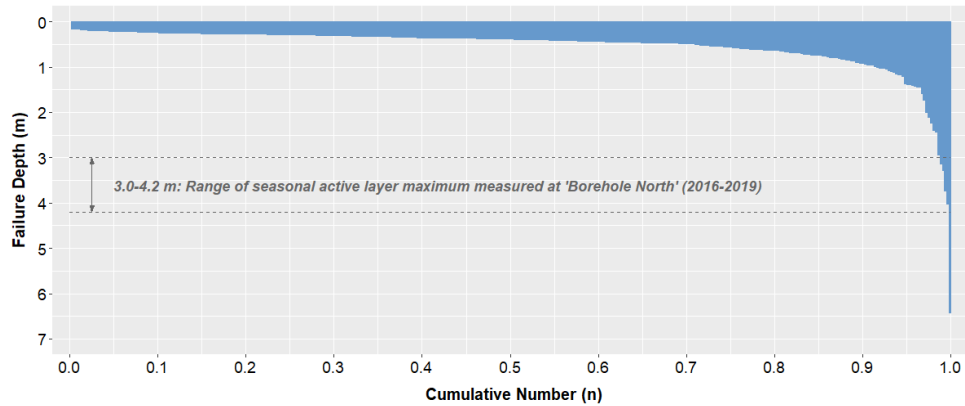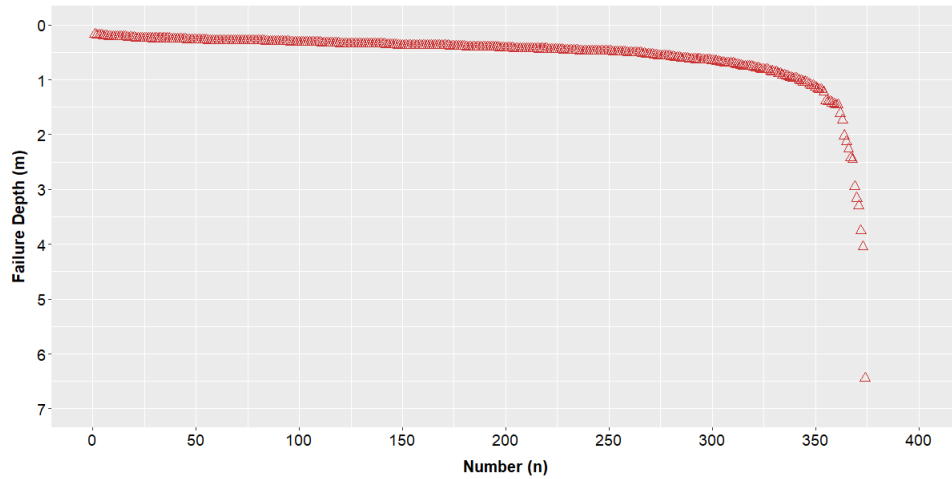
31

Figure 138: **Failure depths** ~~Depth of detachment plane~~ **for all registered rockfalls (**n = 374~~> 0.1 m³~~**). More than 90 % of all rockfalls failed within less than 1 m from the surface.** **The seasonal active layer maximum measured at T-BN (30 m deep borehole at KN) ranged from 3.0-4.2 m (2016-2019).**

715

720

Table 2: Rockfalls with failure depths > 1 m and > 2 m classified by slope aspect. Rockfalls with failure depths > 1 m (> 2 m) are most frequent in W-, SE- and N-facing rockwall sections.

Slope Aspect	Failure Depth > 1 m		Failure Depth > 2 m	
	Total Number (n)	*Normalised Number (n per 10,000 m^2 per a)*	*Total Number (n)*	*Normalised Number (n per 10,000 m^2 per a)*
N	8	0.34	2	0.09
NE	-	-	-	-
E	2	0.08	1	0.04
SE	8	1.07	3	0.40
S	-	-	-	-
SW	-	-	-	-
W	5	1.24	3	0.71
NW	10	0.16	2	0.03

4.7 Bedrock Temperature

Temperatures recorded at the two deep boreholes (T-BN, T-BW) clearly indicate permafrost conditions. From 2016-19 the seasonal maximum active layer thickness at T-BN varied between 3.0 and 4.2 m (Fig. 14). Active layer formation usually starts in late May, maximum thickness is reached in early September, and complete freezing occurs in early or mid-October. Repeated lightning strike damage resulted in fragmentary data recording at T-BW and hinders full seasonal characterisation of active layer evolution. Seasonal temperature variations at T-BN occur down to a depth of 15-20 m, below which a constant temperature of -1.8 °C was observed over the entire period. At the Kitzsteinhorn W-face (T-BW) temperature at 25 m borehole depth ranged between -1.1 to -1.2 °C (Fig. S3) and comparable values are expected to occur also at E-oriented rockwalls in the study area, given similar topo-climatic conditions at W- and E-faces (Schrott et al., 2012).

Shallow bedrock temperatures measured at 0.8 m borehole depth (1.0 m at T-BN) demonstrate significant contrasts between the Randkluft (T-RK2, T-RK3) and the open rockwall (T-BN, T-MKE) (Fig. 15), and indicate a pronounced modification of the ground thermal regime after deglaciation. Temperatures inside the Randkluft remained slightly below or at 0 °C during the entire observation period and show near-isothermal behaviour with annual variations of just around 1 K (Table 3). Significant, short-term autumn cooling through advection of cold air into the open Randkluft was registered only once (Oct 2016) and during the winter season a slow, long-term cooling trend was observed, which ends abruptly in late spring (May/Jun) most likely through extensive percolation of meltwater into the Randkluft. Large seasonal amplitudes around 20 K were recorded in the open rockwall where temperatures ranged from -12 to +6 °C at the N-facing T-BN, and from -12 to +12 °C at the warmer ESE-facing T-MKE. Seasonal amplitudes at the Randkluft aperture (T-RK1) varied between 7 and 9 K over the four-year monitoring period.

Kommentiert [IH41]: Table added following suggestion by RC1 (A. Anders).
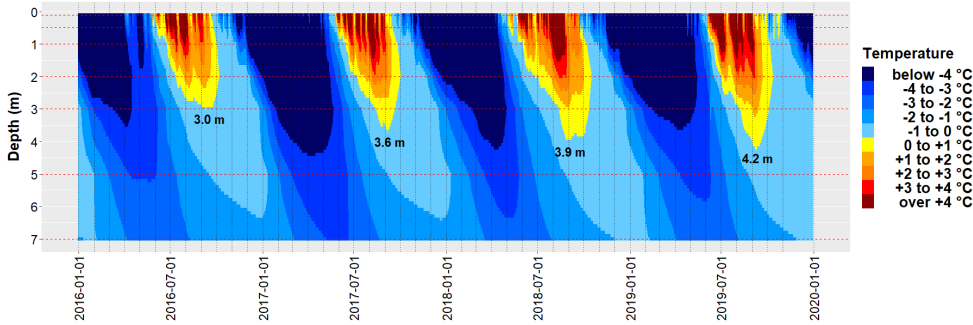
RC1 (A. Anders) wrote:
"Is there a difference in the thickness of the rockfalls with orientation (or a pattern related to location)?"

Kommentiert [IH42]: Subchapter added following suggestions by RC1 (A. Anders), SC1 (J. Beutel) and RC2 (R. Kenner) who all asked for a more thorough thermal characterisation of the studied rockwalls.

Figure 14: Four-year borehole temperature record from 30 m deep borehole T-BN (2,985 m a.s.l.) located at Kitzsteinhorn north-face (KN) (first 7 m are displayed). The seasonal maximum of the active layer (indicated on plot) ranged from 3.0-4.2 m.
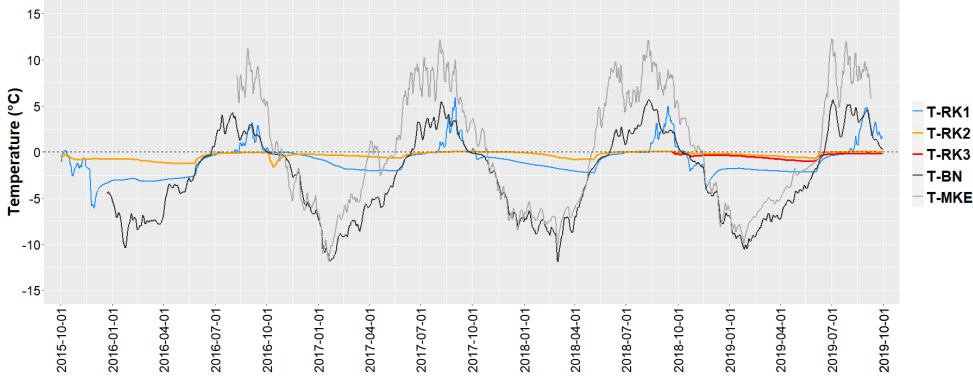
Figure 15: Near-surface bedrock temperature for five measurement sites located at Kitzsteinhorn north-face (KN) and Magnetkoepfl east-face (MKE). Perennially-frozen, near-isothermal conditions observed inside the Randkluft (T-RK2, T-RK3) contrast with large seasonal amplitudes in the open rockwall. All temperatures were measured at 0.8 m borehole depth (1.0 m at T-BN).

Table 3: Annual mean, minimum, and maximum near-surface bedrock temperature for five measurement sites at Kitzsteinhorn north-face (KN) and Magnetkoepfl east-face (MKE).

Site	Elev.	Aspect	2015/2016 *1 Oct – 30 Sep*				2016/2017 *1 Oct – 30 Sep*				2017/2018 *1 Oct – 30 Sep*				2018/2019 *1 Oct – 30 Sep*			
	m.a.s.l.		Mean °C	Min. °C	Max. °C	Diff. °C	Mean °C	Min. °C	Max. °C	Diff. °C	Mean °C	Min. °C	Max. °C	Diff. °C	Mean °C	Min. °C	Max. °C	Diff. °C
T-RK1	2,906	NE	-1.7	-6.1	3.2	9.3	-0.5	-2.1	5.9	8.0	-0.6	-2.3	5.0	7.3	-1.0	-3.9	4.9	8.8
T-RK2	2,899	NE	-0.6	-1.3	0.0	1.3	-0.3	-1.6	0.1	1.7	-0.2	-0.8	0.1	0.9	-0.2	-0.7	0.1	0.8
T-RK3	2,892	NE	-	-	-	-	-	-	-	-	-	-	-	-	-0.5	-1.0	-0.1	0.9
T-BN	2,985	N	-	-	-	-	-2.8	-11.9	5.5	17.4	-2.5	-11.9	5.7	17.6	-2.7	-10.5	5.7	16.2
T-MKE	2,902	ESE	-	-	-	-	0.2	-11.6	12.2	23.8	0.1	-10.3	12.1	22.4	-0.6	-9.9	12.3	22.2

5 Discussion

755 The analysis of long-term terrestrial LiDAR data from two high-alpine cirques shows that rockfall source areas are grouped along heavily fractured, pre-existing structural weaknesses (Sect. 4.2), in accordance ~~which is consistent~~ with former studies that found correlations between ~~joint density~~ fracturing and rockwall retreat (Sass, 2005; Moore et al., 2009). Sectoral analyses of (normalised) rockfall activity demonstrate increased volumes, numbers and deeper failure plains in N-, W- and SE-facing slopes (Sect. 4.6), which is consistent with the orientations of major discontinuities at the study site. Steep joint sets (J1, J2)
760 facilitate large detachments in W- and SE-oriented terrain, while strike and dip of the micaschist cleavage promote frequent dip-slope failures in N-facing rockwall sections. Particularly the latter mode of failure may represent a key mechanism of cirque expansion as pronounced north-south elongated cirque morphologies at the Kitzsteinhorn indicate effective cleavage-driven headwall sapping over long time-scales (Hartmeyer et al., 2020).

Further analysis reveals considerably increased rockfall activity in the immediate proximity (10-20 vertical meters) of the
765 current glacier surface, which emerged from the ice only very recently. While some of the increase may be related to a slight steepening of rockwall gradients towards the glacier surface, a number of other processes are likely responsible for the observed glacier-proximal rockfall increase.

5.1 Antecedent Rockfall Preparation inside the Randkluft

Slope debuttressing following deglaciation is frequently considered to cause mass movements, particularly in case of larger
770 slope failures. (e.g. Holm et al., 2004; Allen et al., 2010). At the base of the investigated rockwalls, however, seasonally air- or snow-filled voids between glacier and cirque wall ('Randkluft') prevent permanent physical contact between rock and ice and thus effectively hinder debuttressing. The existence of a Randkluft is not site-specific but rather common at alpine (cirque) glaciers (e.g. Gardner, 1987; Mair and Kuhn, 1994; Sanders et al., 2012). Among the rockwalls investigated here, Randkluft systems are most pronounced below KN, possibly due to the principal flow direction of the adjacent glacier perpendicularly
775 away from the slope. Randkluft development is rather limited at KNW, likely caused by substantial (avalanche) snow accumulation at the foot of the tall, low-gradient rockwall.

Local Randkluft systems at the Kitzsteinhorn are usually open during late summer/early fall (Fig. ~~9~~16A), even though Randkluft width and depth exhibit considerable interannual variations. It is evident from our observations that the debuttressing effect, if relevant at all (McColl, 2012; McColl and Davies, 2012), can occur subglacially only, in the lowermost parts of the
780 Randkluft. Sporadically, the collapse of ice bridges may cause small-scale debuttressing locally, but in general this mode of failure seems not too effective. Debuttressing can also not explain the increased rockfall activity several meters above the glacier surface, i.e. in areas already ice-free for years or decades.

Kommentiert [IH43]: Existing paragraph expanded following suggestions by RC1 (A. Anders) and SC1 (J. Beutel) who criticised missing information the influence of weakness zones and geological structure.
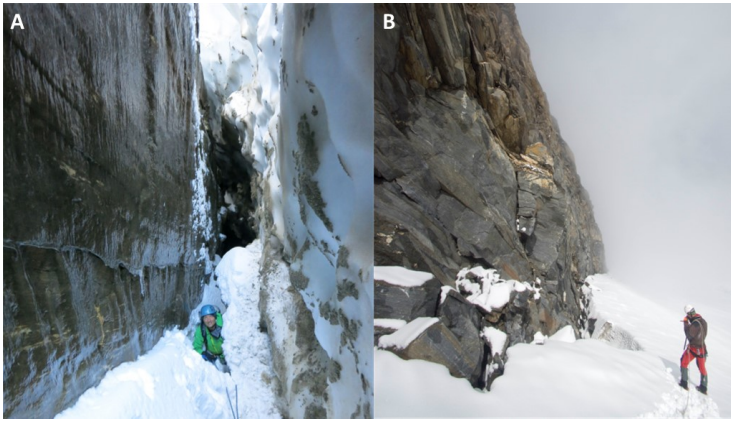
785   **Figure 16̶9A: Inside the Randkluft below KN (Kitzsteinhorn north-face). Pictured person is standing approximately 8 m below the glacier surface. Continuous ice coating (verglas) on the cirque wall (left half of the photo) indicates permanently frozen conditions inside the Randkluft (Photo: Ingo Hartmeyer, 09.10.2015). 16B: Magnetkoepfl east-face (MKE) and adjacent glacier separated by Randkluft. Recently deglaciated, unstable blocks are visible in the first meters above the glacier surface. Occasionally rockfall deposits are wedged between rockwall and Randkluft lip (bottom left) (Photo: Robert Delleske, 04.09.2015).**

790 ~~Previous modelling approaches assume unfrozen conditions for currently glacier-covered, north-facing headwall sections and aggradation of new permafrost after deglaciation (Wegmann et al., 1998).~~ Direct observations from Randkluft environments are scarce and have so far relied on visual evidence (Johnson, 1904) and some in-situ air temperature records (Battle and Lewis, 1951). Assessments of the thermal regime range from freeze/thaw-dominated conditions (Johnson, 1904) to stable sub-

795 zero conditions (Gardner, 1987). Here, we report a first set of bedrock temperatures from a Randkluft: four-year records from shallow boreholes (0.8 m deep) located 7 m and 14 m below glacier surface (Sect. 4.7). Temperatures remain at or just below 0 °C during the entire observation period and display extremely low seasonal variability (~ 1 K). We visually observed significant melt- and rainwater runoff from the rockwall into the Randkluft during the summer season. Below Randkluft depths of 5 to 10 m rockwalls were covered in thick layers of refrozen water ('verglas') that persisted during the entire observation period (Fig. S2).

800 ~~Other studies report distinct permafrost conditions inside Randkluft systems based on in-situ temperature measurements (Sanders et al., 2012). Our observations match with the latter findings, as we encountered rockwalls coated with refrozen meltwater ('verglas') as deep as 15 m below the glacier surface during late summer (Fig. 9).~~ The existence of ~~p~~Perennially frozen conditions inside the Randkluft ~~in~~ combin~~ation~~ed with ~~the~~observed extensive ~~melt~~water supply from the rockwall above may significantly ~~contribute to~~ increase the efficacy of frost weathering in such subglacial cirque wall sections. One of the few

805 quantitative studies indicates particularly effective rock-fracturing driven by ice segregation within the Randkluft of a temperate glacier in British Columbia, Canada (Sanders et al., 2012). This observation has recently been substantiated by numerous field and lab experiments demonstrating intense frost cracking by ice segregation at temperatures just below 0 °C (Girard et al., 2013; Duca et al., 2014; Murton et al., 2016) and thermo-cryogenic rock fatigue due to damage accumulation over longer time scales (Jia et al., 2015). Subcritical stress propagation due to ice segregation driven by sustained freezing and

810 sufficient water supply (Jia et al., 2017; Draebing and Krautblatter, 2019), and high ~~plucking~~quarrying-related tensile stresses caused by refreezing meltwater at the bottom of the Randkluft (Lewis, 1938; Hooke, 1991) are therefore~~. We~~ hypothesi~~z~~sed ~~to be, therefore, that they are~~ the dominant antecedent processes of rockfall preparation. The special weathering conditions may prepare the high fragmentation of near-Randkluft bedrock which efficiently predisposes cirque walls to shallow failures and ultimately controls the high post-glacial rockfall activity. ~~This idea is further underpinned by a possible positive correlation~~

815 ~~between Randkluft size and glacier-proximal rockfall volume. Highest proximal rockfall volumes are found at KN and MKE which also host the largest Randkluft systems of all rockwalls monitored. Lowest proximal rockfall volumes are recorded at KNW where Randkluft formation is suppressed due to massive local snow accumulation at the glacier fringe.~~ Observations made in the present study contribute to a more than one century long discussion on the mechanisms of cirque headwall retreat (Richter, 1900; Martonne, 1901). Earlier studies postulate high erosion at the base of the headwall to account

820 for the development of the characteristic break of slope (schrundline) and a low-gradient cirque floor (Evans, 1997). We found smooth, vertical rockwall sections inside the Randkluft (Fig. 16A) that do not match the cataclinal headwall morphology above the glacier (~ 45° slope following the direction of cleavage), confirming a vastly different erosion regime at the ice-covered headwall base. Furthermore, the observed ample water supply and refreezing in the narrow, lower Randkluft sections may

Kommentiert [IH46]: This paragraph was expanded/modified to briefly discuss the newly included temperature data.

Kommentiert [IH47]: Slightly modified following suggestion by RC2 (R. Kenner).

RC2 (R. Kenner) wrote:
"Important for subglacial rock weathering within a Bergschrund is probably ice-segregation but this is not even mentioned."

Kommentiert [IH48]: Deleted following suggestion by RC2 (R. Kenner).

RC2 (R. Kenner) wrote:
"This is very speculative. I do not see a sound argumentation here."

37

efficiently strengthen the bond between headwall and glacier ice and thus promote erosion by quarrying, leading to localised erosion at the lower headwall (Hooke, 1991).

5.2 Deglaciation-Induced Thermomechanical Forcing and Active Layer Formation

As glaciers are wasting down, boundary conditions at freshly exposed rockwall sections are shifted from subglacial to subaerial boundary conditions. The thermal effects of this transition – quantified here for the very first time – are drastic as ground thermal conditions emerge from a near-isothermal, subglacial setting and convert to a strongly seasonal regime. A modification clearly justifying its recent designation as 'paraglacial thermal shock' (Grämiger et al., 2018). The quantitative effects of this transition are elusive, as direct measurements from subglacial cirque wall sections are rare (Gardner, 1987; Sanders et al., 2012). Yet it is expected that thermal conditions in cirque walls are modified significantly as they emerge from isothermal, subglacial conditions – a transition that has recently been named 'paraglacial thermal shock' (Grämiger et al., 2018). Once ice-free, the measured strong diurnal and seasonal variations are likely to induce pronounced thermal stress leading to deformation (Hasler et al., 2012; Weber et al., 2017) and potentially to failure along critically-stressed discontinuities (Hall, 1999; Gischig et al., 2011). Additionally, cyclic freeze-thaw action will cause rock fatigue (Jia et al., 2015), hydrofracture (Davidson and Nye, 1985; Sass, 2004) and the expansion of water-filled joints (Matsuoka and Murton, 2008), all of which promote destabilization in recently deglaciated rockwall sections (Draebing et al., 2017).

Active layer deepening – a key element of permafrost degradation (Ravanel et al., 2017) – significantly alters rock- and ice-mechanical properties (Davies et al., 2001; Krautblatter et al., 2013) and is frequently considered in high-alpine rockfall analyses (e.g. Gruber and Haeberli, 2007; Weber et al., 2019). Failure depth of rockfalls related to permafrost degradation is expected to equal or exceed maximum active layer thickness. At a local borehole monitoring site at KNin a N-facing rockwall section (T-BN) the active layer depth varies between around 3 to 4 m inter-annually. Based on these values, only 0.5 % (below 4 m) to 1.3 % (below 3 m) of all rockfalls failed at a depth below the maximum seasonal active layer. Volume shares are significantly higher due to the large size of the deeper-seated events: Rockfalls with failure depths larger than 3 m (4 m) constitute 44 % (60 %) of the total rockfall volume, suggesting that permafrost degradation could indeed have a substantial impact on total rockfall volume.

Active layer thickness is expected to vary strongly across the investigated rockwalls (Schrott et al., 2012), mainly due to slope aspect (Schrott et al., 2012), topography effects (Gruber et al., 2004), and snow cover variations (Haberkorn et al., 2015). Active layer depth monitored at a single borehole (at KNT-BN) is therefore unlikely to be representative for the entire study area. Temperature measurements at T-BW and T-MKE confirm this assumption and point to larger active layer depths at W- and E-facing rockwalls. Particularly for recently deglaciated rockwall sections, permafrost dynamics are poorly understood due to the complex local interplay of glaciological, meteorological and geological controls (Draebing et al., 2014). Observations point at the complete absence of an active layer in glacier-covered rockwall sections (Fig. 9). Bedrock temperatures measured inside the Randkluft (T-RK2, T-RK3) below a NE-facing rockwall demonstrate temperatures below or at 0 °C and the complete absence of an active layer. At the Randkluft aperture (i.e. at the level of the glacier surface) a short

1-2 month time-window with positive temperatures was recorded indicating the formation of a shallow active layer. Glacial downwasting ~~would thus~~ uncovers permanently frozen rockwalls and causes the formation of an incipient active layer, which is likely initiated in the uppermost metres of the Randkluft. This process is expected to ~~have a significant destabilizing effect~~ alter rock- and ice-mechanical properties (Davies et al., 2001; Krautblatter et al., 2013), promote the infiltration of water (Gruber and Haeberli, 2007; Hasler et al., 2011), and ~~may~~ will therefore contribute considerably to the increased rockfall activity near the current glacier surface.

Further influences that potentially contribute to high glacier-proximal rockfall activity, include late-spring ground avalanches and channelized rainwater runoff after heavy precipitation. Visual observation suggests strong erosive effects for these processes in the freshly deglaciated sections where blocks at failure stability limit are abundant (Fig. 16B~~9~~). More precise quantification of such processes would require significantly shorter survey return periods.

~~Figure 10: Magnetkoepfl east-face (MKE) and adjacent glacier separated by Randkluft. Recently deglaciated, unstable blocks are visible in the first meters above the glacier surface. Occasionally rockfall deposits are wedged between rockwall and Randkluft lip (bottom left) (Photo: Robert Delleske, 04.09.2015).~~

Kommentiert [IH50]: Modified following suggestion by RC2 (R. Kenner).

RC2 (R. Kenner) wrote:
"You should mention the infiltration of water after AL formation what is one of the key game changers."

Kommentiert [IH51]: This paragraph was expanded/modified to briefly discuss the newly included temperature data.

Kommentiert [IH52]: Old Fig. 9 and 10 were merged into new Fig. 16A and 16B

6 Conclusions

We present a unique rockfall inventory from a six-year terrestrial LiDAR campaign (2011-2017) for permafrost-affected rockwalls of two glaciated cirques in the Central Alps of Austria (Kitzsteinhorn). The five rockwalls studied are all influenced by significant glacial downwasting and ice-~~apron~~face degradation. We draw the following conclusions:

875

- The inventory represents the most extensive dataset of high-alpine rockfall to date and the first quantitative documentation of a cirque-wide erosional response of glaciated rockwalls to recent climate warming.

- During the monitoring period 632 rockfalls with an overall volume of 2,564.3 ± ~~1.5~~141.9 m³ were recorded. In addition, 113 rockfall source areas with a total volume of 292.0 ± 72.3~~0.4~~ m³ were detected in unconsolidated sediments. Mass loss from ice-~~apron~~face degradation accounted for an overall volume of 575.9 ± ~~0.04~~73.9 m³.

880

- Rockfall activity concentrates along pre-existing structural weaknesses and was highest in recently deglaciated areas: 60 % of the rockfall volume originated from source areas located fewer than ten vertical meters above the current glacier surface; 75 % detached within 20 vertical meters of the glacier surface.

- Increased mass wasting activity in recently deglaciated areas, such as discovered in the present study, is typical of paraglacial environments, where slope systems gravitationally adjust to new, non-glacial boundary conditions.

885

- Previous studies on the paraglacial adjustment of bedrock slopes mostly focused on high-magnitude events such as rock avalanches and rockslides, which commonly respond to deglaciation on centennial to millennial time scales. The lower end of the paraglacial magnitude-frequency spectrum is currently poorly characterized. The present study bridges this gap and for the first time provides field evidence of an immediate, low-magnitude paraglacial response in a currently deglaciating rock slope system.

890

- Distinct Randklufts, which separate the investigated cirque walls from the adjacent glacial ice, effectively prevent debuttressing. To characterise the thermal regime of the Randkluft we carried out unprecedented shallow borehole (0.8 m) measurements at 7 and 14 m Randkluft depth, and found ~~Inside the Randkluft we observed~~ perennially frozen conditions and extensive refreezing of meltwater supplied from the rockwall above.

- Sustained freezing along with sufficient water availability in the Randkluft likely drive subcritical stress propagation by ice segregation and cause high ~~plucking~~quarrying-related tensile stresses, which contribute to antecedent rockfall preparation when the rockwall is still ice-covered.

895

- As the glacier is wasting down strong diurnal and seasonal temperature variations induce pronounced thermal stress, cause rock fatigue and lead to the first-time formation of an active layer, which is expected to exert a significant destabilizing effect on glacier-proximal areas.

900 **Data availability.** The rockfall inventory can be downloaded from the *mediaTUM* data repository under the following weblink: https://mediatum.ub.tum.de/1540134. Terrestrial LiDAR data is available on request.

Supplement. The supplement is provided in a separate file.

Kommentiert [IH53]: Modified following suggestion of RC2 (R. Kenner) to more explicitly consider the role ice segregation.

Kommentiert [IH54]: Modified following suggestion by SC1 (J. Beutel)

SC1 (J. Beutel) wrote:
"Is the LIDAR (airborne and terrestrial) available? or can it be made available`?"

References

Abellán, A., Vilaplana, J. M., Calvet, J., García-Sellés, D., and Asensio, E.: Rockfall monitoring by Terrestrial Laser Scanning – case study of the basaltic rock face at Castellfollit de la Roca (Catalonia, Spain), NAT HAZARD EARTH SYS, 11(3), 829-841, 2011.

Akca, D.: Least Squares 3D Surface Matching, Ph.D. thesis, Swiss Federal Institute of Technology Zurich, 2007.

Allen, S. K., Cox, S. C., and Owens, I. F.: Rock avalanches and other landslides in the central Southern Alps of New Zealand: a regional study considering possible climate change impacts, LANDSLIDES, 8(1), 33-48, 2010.

Auer, I., Foelsche, U., Böhm, R., Chimani, B., Haimberger, L., Kerschner, H., Koinig, K. A., Nicolussi, K., and Spötl, C.: Vergangene Klimaänderung in Österreich, in: Österreichischer Sachstandsbericht Klimawandel 2014 (AAR14), edited by: Kromp-Kolb, H., Nakicenovic, N., Steininger, K., Gobiet, A., Formayer, H., Köppl, A, Prettenthaler, F., Stötter, J., and Schneider, J., Verlag der Österreichischen Akademie der Wissenschaften, Vienna, Austria, 227-300, 2014.

Augustinus, P. C.: Glacial valley cross-profile development: the influence of in situ rock stress and rock mass strength, with examples from the Southern Alps, New Zealand, GEOMORPHOLOGY, 14(2), 87-97, 1995.

Ballantyne, C. K.: Paraglacial geomorphology, QUATERNARY SCI REV, 21(18-19), 1935-2017, 2002.

Ballantyne, C. K., Sandeman, G. F., Stone, J. O., and Wilson, P.: Rock-slope failure following Late Pleistocene deglaciation on tectonically stable mountainous terrain, QUATERNARY SCI REV, 86, 144-157, 2014.

Barlow, J., Lim, M., Rosser, N., Petley, D., Brain, M., Norman, E., and Geer, M.: Modeling cliff erosion using negative power law scaling of rockfalls, GEOMORPHOLOGY, 139-140, 416-424, 2012.

41

Barnhart, T. B. and Crosby, B. T.: Comparing Two Methods of Surface Change Detection on an Evolving Thermokarst Using High-Temporal-Frequency Terrestrial Laser Scanning, Selawik River, Alaska, Remote Sensing, 5, 2813-2837, 2013.

935 Battle, W. R. B. and Lewis, W. V.: Temperature observations in bergschrunds and their relationship to cirque erosion, Journal of Geology, 59, 537–545, 1951.

Benn, D. I. and Evans, D. J. A.: Glaciers & Glaciation, Routledge Taylor & Francis Group, London and New York, 2010.

Besl, P. J. and McKay, N. D.: A method for registration of 3-D shapes, IEEE T PATTERN ANAL, 14(2), 239-256, 1992.

Böhm, R.: Changes of regional climate variability in central Europe during the past 250 years, EUR PHYS J PLUS, 127(5),
940 2012.

Chen, Y. and Medioni, G.: Object modelling by registration of multiple range images, IMAGE VISION COMPUT, 10(3), 145-155, 1992.

Church, M. and Ryder, J.: Paraglacial Sedimentation: A Consideration of Fluvial Processes Conditioned by Glaciation, GEOL SOC AM BULL, 83(10), 3059, 1972.

945 Cook, K.: An evaluation of the effectiveness of low-cost UAVs and structure from motion for geomorphic change detection, GEOMORPHOLOGY, 278, 195-208, 2017.

Cornelius, H. and Clar, E.: Erläuterungen zur geologischen Karte des Glocknergebietes, Geologische Bundesanstalt, Vienna, 32 pp., 1935.

Cossart, E., Braucher, R., Fort, M., Bourlès, D. L., and Carcaillet, J.: Slope instability in relation to glacial debuttressing in
950 alpine areas (Upper Durance catchment, southeastern France): Evidence from field data and 10Be cosmic ray exposure ages, GEOMORPHOLOGY, 95(1-2), 3-26, 2008.

Davidson, G. P. and Nye, J. F.: A photoelastic study of ice pressure in rock cracks, COLD REG SCI TECHNOL, 11(2), 141-153, 1985.

Davies, M. C. R., Hamza, O., and Harris, C.: The effect of rise in mean annual temperature on the stability of rock slopes
955 containing ice-filled discontinuities, PERMAFROST PERIGLAC, 12(1), 137-144, 2001.

de Haas, T., Conway, S. J., and Krautblatter, M.: Recent (Late Amazonian) enhanced backweathering rates on Mars: Paracratering evidence from gully alcoves, J GEOPHYS RES-PLANET, 120(12), 2169-2189, 2015.

Deline, P., Kirkbride, M. P., Ravanel, L., and Ravello, M.: The Trê-la-Tête rockfall onto the Glacier de la Lex Blanche, Mont Blanc Massif, Italy, in September 2008, GEOGR FIS DIN QUAT, 31(2), 251-254, 2008.

960 Deline, P.: Interactions between rock avalanches and glaciers in the Mont Blanc massif during the late Holocene, QUATERNARY SCI REV, 28(11-12), 1070-1083, 2009.

Delmas, M., Calvet, M., and Gunnell, Y.: Variability of Quaternary glacial erosion rates – A global perspective with special reference to the Eastern Pyrenees, QUATERNARY SCI REV, 28(5-6), 484-498, 2009.

Draebing, D., Krautblatter, M., and Dikau, R.: Interaction of thermal and mechanical processes in steep permafrost rock walls:
965 A conceptual approach, GEOMORPHOLOGY, 226, 226-235, 2014.

Draebing, D., Krautblatter, M., and Hoffmann, T.: Thermo-cryogenic controls of fracture kinematics in permafrost rockwalls, GEOPHYS RES LETT, 44(8), 3535-3544, 2017.

Draebing, D. and Krautblatter, M.: The Efficacy of Frost Weathering Processes in Alpine Rockwalls, GEOPHYS RES LETT, 46(12), 6516-6524, 2019.

Duca, S., Occhiena, C., Mattone, M., Sambuelli, L., and Scavia, C.: Feasibility of Ice Segregation Location by Acoustic Emission Detection: A Laboratory Test in Gneiss, PERMAFROST PERIGLAC, 25(3), 208-219, 2014.

Dussauge-Peisser, C., Helmstetter, A., Grasso, J.-R., Hantz, D., Desvarreux, P., Jeannin, M., and Giraud, A.: Probabilistic approach to rock fall hazard assessment: potential of historical data analysis, NAT HAZARD EARTH SYS, 2, 15-26, 2002.

Esposito, G., Salvini, R., Matano, F., Sacchi, M., Danzi, M., Somma, R., and Troise, C.: Multitemporal monitoring of a coastal landslide through SfM-derived point cloud comparison, The Photogrammetric Record, 32, 459-479, 2017.

Evans, I. S.: Process and form in the erosion of glaciated mountains, in: Process and Form in Geomorphology, edited by: Stoddart, D. R., Routledge, London, 145–174, 1997.

Ewald, A., Hartmeyer, I., Keuschnig, M., Lang, A., and Otto, J.-C.: Fracture Dynamics In An Unstable, Deglaciating Headwall, Kitzsteinhorn, Austria, EGU General Assembly, Vienna, Austria, 7–12 April 2019, EGU2019-3055, 2019.

Fischer, A., Olefs, M., and Abermann, J.: Glaciers, snow and ski tourism in Austria's changing climate, ANN GLACIOL, 52(58), 89-96, 2011a.

Fischer, L., Kääb, A., Huggel, C., and Noetzli, J.: Geology, glacier retreat and permafrost degradation as controlling factors of slope instabilities in a high-mountain rock wall: the Monte Rosa east face, NAT HAZARD EARTH SYS, 6(5), 761-772, 2006.

Fischer, L., Eisenbeiss, H., Kääb, A., Huggel, C., and Haeberli, W.: Monitoring topographic changes in a periglacial high-mountain face using high-resolution DTMs, Monte Rosa East Face, Italian Alps, PERMAFROST PERIGLAC, 22(2), 140-152, 2011b.

Gardner, J. S.: Evidence for Headwall Weathering Zones, Boundary Glacier, Canadian Rocky Mountains, J GLACIOL, 33(113), 60-67, 1987.

Girard, L., Gruber, S., Weber, S., and Beutel, J.: Environmental controls of frost cracking revealed through in situ acoustic emission measurements in steep bedrock, GEOPHYS RES LETT, 40(9), 1748-1753, 2013.

Gischig, V. S., Moore, J. R., Evans, K. F., Amann, F., and Loew, S.: Thermomechanical forcing of deep rock slope deformation: 1. Conceptual study of a simplified slope, J GEOPHYS RES-EARTH, 116(F4), 2011.

Grämiger, L., Moore, J. R., Gischig, V. S., Ivy-Ochs, S., and Loew, S.: Beyond debuttressing: Mechanics of paraglacial rock slope damage during repeat glacial cycles, J GEOPHYS RES-EARTH, 122(4), 1004-1036, 2017.

Grämiger, L., Moore, J. R., Gischig, V. S., and Loew, S.: Thermomechanical Stresses Drive Damage of Alpine Valley Rock Walls During Repeat Glacial Cycles, J GEOPHYS RES-EARTH, 123(10), 2620-2646, 2018.

Grant, D., Bethel, J., and Crawford, M.: Point-to-plane registration of terrestrial laser scans, ISPRS J PHOTOGRAMM, 72, 16-26, 2012.

43

Gruber, S., Hoelzle, M., and Haeberli, W.: Rock-wall temperatures in the Alps: modelling their topographic distribution and regional differences, PERMAFROST PERIGLAC, 15(3), 299-307, 2004.

Gruber, S., and Haeberli, W.: Permafrost in steep bedrock slopes and its temperature-related destabilization following climate change, J GEOPHYS RES-EARTH, 112(F2), 2007.

Haberkorn, A., Phillips, M., Kenner, R., Rhyner, H., Bavay, M., Galos, S. P., and Hoelzle, M.: Thermal regime of rock and its relation to snow cover in steep alpine rock walls: Gemsstock, Central Swiss Alps, GEOGR ANN A, 97(3), 579-597, 2015.

Haeberli, W., Hoelzle, M., Paul, F., and Zemp, M.: Integrated monitoring of mountain glaciers as key indicators of global climate change: the European Alps, ANN GLACIOL, 46, 150-160, 2007.

Hales, T. C. and Roering, J. J.: A frost "buzzsaw" mechanism for erosion of the eastern Southern Alps, New Zealand, GEOMORPHOLOGY, 107(3-4), 241-253, 2009.

Hall, K.: The role of thermal stress fatigue in the breakdown of rock in cold regions, GEOMORPHOLOGY, 31(1-4), 47-63, 1999.

Hallet, B., Walder, J. S., and Stubbs, C. W.: Weathering by segregation ice growth in microcracks at sustained subzero temperatures: Verification from an experimental study using acoustic emissions, PERMAFROST PERIGLAC, 2(4), 283-300, 1991.

Hartmeyer, I., Keuschnig, M., and Schrott, L.: A scale-oriented approach for the long-term monitoring of ground thermal conditions in permafrost-affected rock faces, Kitzsteinhorn, Hohe Tauern Range, Austria, AUSTRIAN J EARTH SCI, 105(2), 128-139, 2012.

Hartmeyer, I., Keuschnig, M., Delleske, R., Krautblatter, M., Lang, A., Schrott, L., and Otto, J.-C.: Enhanced rockwall retreat and modified rockfall magnitudes/frequencies in deglaciating cirques from a 6-year LiDAR monitoring, EARTH SURF DYNAM, 2020submitted.

Hasler, A., Gruber, S., Font, M., and Dubois, A.: Advective Heat Transport in Frozen Rock Clefts: Conceptual Model, Laboratory Experiments and Numerical Simulation, PERMAFROST PERIGLAC, 22, 378-389, 2011.

Hasler, A., Gruber, S., and Beutel, J.: Kinematics of steep bedrock permafrost, J GEOPHYS RES-EARTH, 117(F01016), 2012.

Hodge, R. A.: Using simulated Terrestrial Laser Scanning to analyse errors in high-resolution scan data of irregular surfaces, ISPRS J PHOTOGRAMM, 65, 227-240, 2010.

Hoeck, V., Pestal, G., Brandmaier, P., Clar, E., Cornelius, H., Frank, W., Matl, H., Neumayr, P., Petrakakis, K., Stadlmann, T., and Steyrer, H.: Geologische Karte der Republik Österreich, Blatt 153 Großglockner, Geologische Bundesanstalt, Vienna, 1994.

Holm, K., Bovis, M., and Jakob, M.: The landslide response of alpine basins to post-Little Ice Age glacial thinning and retreat in southwestern British Columbia, GEOMORPHOLOGY, 57(3-4), pp.201-216, 2004.

Holzhauser, H., Magny, M. J., Zumbühl, H. J.: Glacier and lake-level variations in west-central Europe over the last 3500 years, The Holocene 15, 789–801, 2005.

44

Hooke, R. L.: Positive feedbacks associated with erosion of glacial cirques and overdeepenings, GEOL SOC AM BULL, 103(8), 1104-1108, 1991.

1035 Hormes, A., Müller, B. U., and Schlüchter, C.: The Alps with little ice: evidence for eight Holocene phases of reduced glacier extent in the Central Swiss Alps, HOLOCENE, 11(3), 255-265, 2001.

James, M. R., Robson, S., and Smith, M. W.: 3-D uncertainty-based topographic change detection with structure-from-motion photogrammetry: precision maps for ground control and directly georeferenced surveys, EARTH SURF PROC LAND, 42, 1769-1788, 2017.

1040 Joerin, U. E., Stocker, T. F., Schlüchter, C.: Multicentury glacier fluctuations in the Swiss Alps during the Holocene, The Holocene, 16, 697–704, 2006.

Joerin, U. E., Nicolussi, K., Fischer, A., Stocker, T.F., Schlüchter, C.: Holocene optimum events inferred from subglacial sediments at Tschierva Glacier, Eastern Swiss Alps, Quaternary Science Reviews, 27, 337–350, 2008.

Jia, H., Xiang, W., and Krautblatter, M.: Quantifying Rock Fatigue and Decreasing Compressive and Tensile Strength after
1045 Repeated Freeze-Thaw Cycles, PERMAFROST PERIGLAC, 26(4), 368-377, 2015.

Jia, H., Leith, K., and Krautblatter, M.: Path-Dependent Frost-Wedging Experiments in Fractured, Low-Permeability Granite, PERMAFROST PERIGLAC, 28(4), 698-709, 2017.

Johnson, W. D.: The Profile of Maturity in Alpine Glacial Erosion, The Journal of Geology, 12(7), 569-578, 1904.

Kaser, G., Cogley, J. G., Dyurgerov, M. B., Meier, M. F., and Ohmura, A.: Mass balance of glaciers and ice caps: Consensus
1050 estimates for 1961–2004, GEOPHYS RES LETT, 33(19), 2006.

Kenner, R., Phillips, M., Danioth, C., Denier, C., Thee, P., and Zgraggen, A.: Investigation of rock and ice loss in a recently deglaciated mountain rock wall using terrestrial laser scanning: Gemsstock, Swiss Alps, COLD REG SCI TECHNOL, 67(3), 157-164, 2011.

Keuschnig, M., Hartmeyer, I., Höfer-Öllinger, G., Schober, A., Krautblatter, M., and Schrott, L.: Permafrost-Related Mass
1055 Movements: Implications from a Rock Slide at the Kitzsteinhorn, Austria, in: Engineering Geology for Society and Territory, edited by: Lollino, G., Manconi, A., Clague, J. Shan, W., and Chiarle, M., Springer International Publishing, 1(48), 255-259, 2015.

Keuschnig, M., Krautblatter, M., Hartmeyer, I., Fuss, C., and Schrott, L.: Automated Electrical Resistivity Tomography Testing for Early Warning in Unstable Permafrost Rock Walls Around Alpine Infrastructure, PERMAFROST PERIGLAC,
1060 28(1), 158-171, 2016.

Krautblatter, M., Funk, D., and Günzel, F.: Why permafrost rocks become unstable: a rock-ice-mechanical model in time and space, EARTH SURF PROC LAND, 38(8), 876-887, 2013.

Krautblatter, M. and Moore, J. R.: Rock slope instability and erosion: toward improved process understanding, EARTH SURF PROC LAND, 39(9), 1273-1278, 2014.

1065 Lague, D., Brodu, N., and Leroux, J.: Accurate 3D comparison of complex topography with terrestrial laser scanner: Application to the Rangitikei canyon (N-Z), ISPRS J PHOTOGRAMM, 82, 10-26, 2013.

45

Land Salzburg: Waldstandsaufnahme D, Bild 86-88, 24.08.1953, Salzburger Geographisches Informationssystem (SAGIS), Salzburg, Austria, 1953.

Land Salzburg: Laserscanbefligung Bundesland Salzburg 2008, Salzburger Geographisches Informationssystem (SAGIS), Salzburg, Austria, 2008.

Leith, K., Moore, J. R., Amann, F., and Loew, S.: In situ stress control on microcrack generation and macroscopic extensional fracture in exhuming bedrock, J GEOPHYS RES-SOL EA, 119(1), pp.594-615, 2014.

Lewis, W. V.: A Melt-water Hypothesis of Cirque Formation, GEOL MAG, 75(6), 249-265, 1938.

Mair, R. and Kuhn, M.: Temperature and movement measurements at a bergschrund, J GLACIOL, 40(136), 561-565, 1994.

Manconi, A., Coviello, V., Galletti, M., and Seifert, R.: Short Communication: Monitoring rockfalls with the Raspberry Shake, EARTH SURF DYNAM, 6(4), 1219-1227, 2018.

Martonne, E.: Sur la formation des cirques, ANN GEOGR, 10(49), 10-16, 1901.

Matsuoka, N. and Murton, J. B.: Frost weathering: recent advances and future directions, PERMAFROST PERIGLAC, 19(2), 195-210, 2008.

McColl, S. T. and Davies, T. R. H.: Large ice-contact slope movements: glacial buttressing, deformation and erosion, EARTH SURF PROC LAND, 38(10), 1102-1115, 2012.

Monserrat, O. and Crosetto, M.: Deformation measurement using terrestrial laser scanning data and least squares 3D surface matching, ISPRS J PHOTOGRAMM, 63(1), 142-154, 2008.

Moore, J. R., Sanders, J. W., Dietrich, W. E., and Glaser, S. D.: Influence of rock mass strength on the erosion rate of alpine cliffs, EARTH SURF PROC LAND, 34(10), 1339-1352, 2009.

Murton, J. B., Kuras, O., Krautblatter, M., Cane, T., Tschofen, D., Uhlemann, S., Schober, S., and Watson, P.: Monitoring rock freezing and thawing by novel geoelectrical and acoustic techniques, J GEOPHYS RES-EARTH, 121(12), 2309-2332, 2016.

Naylor, S. and Gabet, E. J.: Valley asymmetry and glacial versus nonglacial erosion in the Bitterroot Range, Montana, USA, GEOLOGY, 35(4), 375, 2007.

Noetzli, J., Huggel, C., Hoelzle, M., and Haeberli, W.: GIS-based modelling of rock-ice avalanches from Alpine permafrost areas, COMPUTAT GEOSCI, 10(2), 161-178, 2006.

Oskin, M. and Burbank, D. W.: Alpine landscape evolution dominated by cirque retreat, GEOLOGY, 33(12), 933, 2005.

Pelto, M. S.: Forecasting temperate alpine glacier survival from accumulation zone observations, CRYOSPHERE, 4(1), 67-75, 2010.

Phillips, M., Wolter, A., Lüthi, R., Amann, F., Kenner, R., and Bühler, Y.: Rock slope failure in a recently deglaciated permafrost rock wall at Piz Kesch (Eastern Swiss Alps), February 2014, EARTH SURF PROC LAND, 42(3), 426-438, 2016.

Plaesken, R., Keuschnig, M., and Krautblatter M.: Systematic derivation of anchoring forces in permafrost-affected bedrock, EGU General Assembly, Vienna, Austria, 23–28 April 2017, EGU2017-14476, 2017.

Purdie, H.: Glacier Retreat and Tourism: Insights from New Zealand, MT RES DEV, 33(4), 463-472, 2013.

Rabatel, A., Deline, P., Jaillet, S., and Ravanel, L.: Rock falls in high-alpine rock walls quantified by terrestrial lidar measurements: A case study in the Mont Blanc area, GEOPHYS RES LETT, 35(10), 2008.

Ravanel, L. and Deline, P.: Climate influence on rockfalls in high-Alpine steep rockwalls: The north side of the Aiguilles de Chamonix (Mont Blanc massif) since the end of the 'Little Ice Age', HOLOCENE, 21(2), 357-365, 2010.

Ravanel, L., Deline, P., Lambiel, C., and Vincent, C.: Instability of a high alpine rock ridge: the lower arête des cosmiques, mont blanc massif, France, GEOGR ANN A, 95(1), 51-66, 2013.

Ravanel, L., Magnin, F., and Deline, P.: Impacts of the 2003 and 2015 summer heatwaves on permafrost-affected rock-walls in the Mont Blanc massif, SCI TOTAL ENVIRON, 609, 132-143, 2017.

Richter, E.: Geomorphologische Untersuchungen in den Hochalpen, PETERMANN GEOGR MITT, 29, 1-103, 1900.

Rosser, N. J., Petley, D. N., Lim, M., Dunning, S. A., and Allison, R. J.: Terrestrial laser scanning for monitoring the process of hard rock coastal cliff erosion, Q J ENG GEOL HYDROGE, 38(4), 363-375, 2005.

Rosser, N. J., Lim, M., Petley, D. N., Dunning, S. A., and Allison, R. J.: Patterns of precursory rockfall prior to slope failure, J GEOPHYS RES-EARTH, 112(F4), 2007.

Sanders, J. W., Cuffey, K. M., Moore, J. R., MacGregor, K. R., and Kavanaugh, J. L.: Periglacial weathering and headwall erosion in cirque glacier bergschrunds, GEOLOGY, 40(9), 779-782, 2012.

Sass, O.: Rock Moisture Fluctuations During Freeze-thaw Cycles: Preliminary Results from Electrical Resistivity Measurements, Polar Geography, 28(1), 13-31, 2004.

Sass, O.: Spatial patterns of rockfall intensity in the northern Alps, Z GEOMORPHOL, 138, 51-65, 2005.

Scherler, D., Bookhagen, B., and Strecker, M. R.: Hillslope-glacier coupling: The interplay of topography and glacial dynamics in High Asia, J GEOPHYS RES-EARTH, 116(F2), 2011.

Schober, A., Bannwart, C., and Keuschnig, M.: Rockfall modelling in high alpine terrain - validation and limitations / Steinschlagsimulation in hochalpinem Raum - Validierung und Limitationen, Geomechanics and Tunnelling, 5(4), 368-378, 2012.

Slupetzky, H. and Ehgartner, G.: Glacier mass balances of Stubacher Sonnblickkees, Hohe Tauern Range, Eastern Alps, Austria, 1958/1959 to 2012/2013. PANGAEA, 2014.

Slupetzky, H.: Die Massenbilanzreihe vom Stubacher Sonnblickkees 1946 bis 2014 und die semidirekte Berechnung des Massenhaushalts von Gletschern, Zeitschrift für Gletscherkunde und Glazialgeologie, 47/48, 167-200, 2015.

Schrott, L., Otto, J.-C., and Keller, F.: Modelling alpine permafrost distribution in the Hohe Tauern region, Austria, AUSTRIAN J EARTH SCI, 105(2), 169-183, 2012.

Solomina, O., Bradley, R. S., Hodgson, D. A., Ivy-Ochs, S., Jomelli, V., Mackintosh, A. N., Nesje, A., Owen, L.A.,Wanner, H., Wiles, G.C., Young, N.E.: Holocene glacier fluctuations, QUATERNARY SCI REV, 111, 9-34, 2016.

Soudarissanane, S., Lindenbergh, R., Menenti, M., and Teunissen, P.: Scanning geometry: influencing factor on the quality of terrestrial laser scanning points, ISPRS Journal of Photogrammetry and Remote Sensing, 66 (4), 389–399, 2011.

Stoffel, M. and Huggel, C.: Effects of climate change on mass movements in mountain environments, PROG PHYS GEOG, 36(3), 421-439, 2012.

Supper, R., Ottowitz, D., Jochum, B., Römer, A., Pfeiler, S., Kauer, S., Keuschnig, M., and Ita, A.: Geoelectrical monitoring of frozen ground and permafrost in alpine areas: field studies and considerations towards an improved measuring technology, NEAR SURF GEOPHYS, 12(1), 93-115, 2013.

Terweh, S.: Geomorphologische Kartierung am Kitzsteinhorn (Hohe Tauern, Österreich) – Eine raum-zeitliche Analyse geomorphologischer Prozesse im Gletscherumfeld des Schmiedingerkees, Bachelor Thesis, University of Bonn, Germany, 67 pp., 2012.

Teza, G., Galgaro, A., Zaltron, N., and Genevois, R.: Terrestrial laser scanner to detect landslide displacement fields: a new approach, INT J REMOTE SENS, 28(16), 3425-3446, 2007.

van Veen, M., Hutchinson, D. J., Kromer, R., Lato, M., and Edwards, T.: Effects of sampling interval on the frequency - magnitude relationship of rockfalls detected from terrestrial laser scanning using semi-automated methods, LANDSLIDES, 14(5), 1579-1592, 2017.

Walder, J. S. and Hallet, B.: A theoretical model of the fracture of rock during freezing, GEOL SOC AM BULL, 96(3), 336, 1985.

Walder, J. S. and Hallet, B.: The Physical Basis of Frost Weathering: Toward a More Fundamental and Unified Perspective, ARCTIC ALPINE RES, 18(1), 27, 1986.

Weber, S., Beutel, J., Faillettaz, J., Hasler, A., Krautblatter, M., and Vieli, A.: Quantifying irreversible movement in steep, fractured bedrock permafrost on Matterhorn (CH), CRYOSPHERE, 11(1), 567-583, 2017.

Weber, S., Beutel, J., Da Forno, R., Geiger, A., Gruber, S., Gsell, T., Hasler, A., Keller, M., Lim, R., Limpach, P., Meyer, M., Talzi, I., Thiele, L., Tschudin, C., Vieli, A., Vonder Mühll, D., and Yücel, M.: A decade of detailed observations (2008–2018) in steep bedrock permafrost at the Matterhorn Hörnligrat (Zermatt, CH), EARTH SYST SCI DATA, 11(3), 1203-1237, 2019.

Wegmann, M., Gudmundsson, G., and Haeberli, W.: Permafrost changes in rock walls and the retreat of alpine glaciers: a thermal modelling approach, PERMAFROST PERIGLAC, 9(1), 23-33, 1998.

Williams, J. G., Rosser, N. J., Hardy, R. J., Brain, M. J., and Afana, A. A.: Optimising 4-D surface change detection: an approach for capturing rockfall magnitude–frequency, EARTH SURF DYNAM, 6(1), 101-119, 2018.

WGMS: Global Glacier Change Bulletin No. 2 (2014-2015), edited by: Zemp, M., Nussbaumer, S. U., Gärtner-Roer, I., Huber, J., Machguth, H., Paul, F., and Hoelzle, M., ICSU(WDS)/IUGG(IACS)/UNEP/UNESCO/WMO, World Glacier Monitoring Service, Zurich, Switzerland, 244 pp., 2017.

Zemp, M., Frey, H., Gärtner-Roer, I., Nussbaumer, S. U., Hoelzle, M., Paul, F., Haeberli, W., Denzinger, F., Ahlstrøm, A. P., Anderson, B., Bajracharya, S., Baroni, C., Braun, L. N., Cáceres, B. E., Casassa, G., Cobos, G., Dávila, L. R., Delgado Granados, H., Demuth, M., Espizua, L., Fischer, A., Fujita, K., Gadek, B., Ghazanfar, A., Ove Hagen, J., Holmlund, P., Karimi, N., Li, Z., Pelto, M., Pitte, P., Popovnin, V. V., Portocarrero, C. A., Prinz, R., Sangewar, C. V., Severskiy, I., Sigurðsson, O.,

Soruco, A., Usubaliev, R., and Vincent, C.: Historically unprecedented global glacier decline in the early 21st century, J GLACIOL, 61(228), 745-762, 2015.